Magnitude and timing of the antiviral response determine SARS-CoV-2 replication early in infection

Nagarjuna R. Cheemarla[1], Timothy A. Watkins[1,2], Valia T. Mihaylova[1], Bao Wang[1,2], Dejian Zhao[3,4], Guilin Wang[3,4], Marie L. Landry[1,5], and Ellen F. Foxman[1,2*]

[1]Department of Laboratory Medicine, [2]Department of Immunobiology, [3]Department of Genetics, [4]Yale Center for Genomic Analysis, and [5]Department of Internal Medicine, Yale School of Medicine, New Haven CT, U.S.A. 06520

*Corresponding author
Correspondence: ellen.foxman@yale.edu

Abstract

The interferon response is a potent antiviral defense mechanism, but its effectiveness in host protection depends on its timing relative to viral replication. Here, we report viral replication and host response kinetics at the start of SARS-CoV-2 infection. Using longitudinal patient nasopharyngeal samples and airway epithelial organoids, we found that SARS-CoV-2 initially replicated exponentially with a doubling time of ~6hr, and induced interferon stimulated genes (ISGs) with delayed kinetics relative to viral replication. Prior exposure to rhinovirus increased ISG levels at the start of SARS-CoV-2 infection and completely blocked SARS-CoV-2 replication. Conversely, inhibiting ISG induction abrogated interference by rhinovirus and increased SARS-CoV-2 replication rate. These results demonstrate the importance of initial interferon-mediated defenses in determining the extent to which SARS-CoV-2 can replicate and indicate that biological variables that alter the airway interferon response could profoundly impact SARS-CoV-2 infection and transmission.

Summary

The interferon response is a potent antiviral defense mechanism, but its effectiveness in host protection depends on its timing relative to viral replication. Here, we report viral replication and host response kinetics at the start of SARS-CoV-2 infection. Using longitudinal patient nasopharyngeal samples and airway epithelial organoids, we found that SARS-CoV-2 initially replicated exponentially with a doubling time of ~6hr, and induced interferon stimulated genes (ISGs) with delayed kinetics relative to viral replication. Prior exposure to rhinovirus increased ISG levels at the start of SARS-CoV-2 infection and completely blocked SARS-CoV-2 replication. Conversely, inhibiting ISG induction abrogated interference by rhinovirus and increased SARS-CoV-2 replication rate. These results demonstrate the importance of initial interferon-mediated defenses in determining the extent to which SARS-CoV-2 can replicate and indicate that biological variables that alter the airway interferon response could profoundly impact SARS-CoV-2 infection and transmission.

Introduction

The novel coronavirus SARS-CoV-2 emerged in late 2019 and has led to a global pandemic, causing over 86M infections and 1.8M deaths at the time of this writing (Dong, 2020). This huge impact has motivated efforts to understand the host immune response to this virus, both to better predict patient outcomes and to design interventions. Innate immune responses can be particularly important for combatting emerging viruses, as these responses do not require prior exposure to effectively defend against a pathogen. While overactivation of the innate immune system late in infection has been recognized as a driver of severe COVID-19 disease, less is known about innate immune responses at the earliest stages of infection when the virus first enters the upper respiratory tract.

A key antiviral defense at mucosal surfaces is the interferon response, initiated when pattern recognition receptors within epithelial cells and immune cells sense general features shared by many viruses, such as common structural features of viral RNA. This recognition event triggers expression of type I and type

III interferons (IFNs) and interferon-stimulated genes (ISGs). Secreted interferons, in turn, bind to cell surface receptors on nearby cells, amplifying ISG expression and creating an antiviral state in the mucosal barrier. Many ISGs encode effectors which directly block viral replication within virus target cells, whereas others encode cytokines which recruit and activate cells of the immune system (Odendall and Kagan, 2015; Schneider et al., 2014).

The role(s) of interferon responses during SARS-CoV-2 infection remain unclear. Recombinant interferon blocks SARS-CoV-2 replication in vitro, and genetic deficiencies in the Type I interferon response as well as anti-interferon autoantibodies have been linked to greater COVID-19 disease severity (Bastard et al., 2020; Lokugamage et al., 2020; Pairo-Castineira et al., 2020; Vanderheiden et al., 2020; Zhang et al., 2020). Furthermore, early data from trials of recombinant Type I or Type III interferon for COVID-19 indicate a therapeutic benefit, particularly when patients are treated early in disease(Feld, 2020; Monk, 2020; Wang, 2020). However, elevated interferon responses later in infection are linked to worse outcomes and may drive immunopathology in severe COVID-19, which generally begins at week two to three of infection, after peak viral replication (Lee and Shin, 2020; Lucas et al., 2020). The literature is mixed about induction of the interferon and ISGs by SARS-CoV-2. While the virus clearly can induce ISG expression in infected epithelia in vitro and in vivo, there is growing evidence that SARS-CoV-2 also antagonizes the interferon response, which may affect the magnitude and timing of the response (Banerjee et al., 2020a, b; Blanco-Melo et al., 2020; Konno et al., 2020; Martin-Sancho et al., 2020; Ravindra et al., 2020; Xia et al., 2020; Zhou et al., 2020). Taken together, these findings suggest that interferons are variably induced during SARS-CoV-2 infection and suggest that host and environmental factors which modulate the timing of this response relative to viral replication may determine whether this response is protective or detrimental. Since a major beneficial function of ISGs is preventing viral replication, the kinetics of the interferon response early in infection are likely to determine its protective impact.

53 One factor that can potentially modulate ISG-mediated defenses in the airway epithelium is recent
54 infection by other viruses, as demonstrated in recent work from our group and others (Essaidi-Laziosi et
55 al., 2020; Wu et al., 2020). Rhinovirus, the most frequent cause of the common cold, is frequently
56 detected in the human upper respiratory tract in the presence and absence of symptoms, and both
57 symptomatic and asymptomatic infections can induce ISG expression in the upper respiratory tract
58 mucosa(Landry and Foxman, 2018; Wolsk et al., 2016; Yu et al., 2019). Therefore, rhinovirus is an
59 example of a common environmental factor which could potentially alter the kinetics of ISG expression
60 at the initial target site of SARS-CoV-2 infection, the airway epithelium.
61
62 Here, we studied the initial host response to SARS-CoV-2 infection and its relationship to viral replication,
63 both in vivo and using an organoid model of the human airway epithelium. Using transcriptomic and
64 biomarker-based analysis of clinical samples and organoid infection experiments, we observed robust
65 ISG induction in the airway mucosa in response to SARS-CoV-2, but also a lag between viral replication
66 and ISG induction. Enhancing ISG expression by prior exposure to a different virus (rhinovirus)
67 profoundly inhibited SARS-CoV-2 replication. Blocking ISG induction completely rescued the effects of
68 interference by rhinovirus and increased replication of SARS-CoV-2 during low MOI infection. These
69 results show the importance of interferon-mediated defenses in restricting SARS-CoV-2 replication and
70 provide an example of how viral interference could impact susceptibility to infection.
71
72 **Results**
73 **Nasopharyngeal host response to SARS-CoV-2 infection identified by RNA-Seq**
74 The host response to SARS-CoV-2 in the upper respiratory tract and its relationship to viral replication
75 are not well-defined. To characterize host responses during SARS-CoV-2 infection in vivo,
76 we performed RNA-Seq on nasopharyngeal (NP) swab RNA from SARS-CoV-2-positive patients (n=30)
77 and SARS-CoV-2-negative healthcare worker controls (n=8). Patients included outpatients and patients
78 admitted to the hospital of both sexes, who ranged in age from 20s to 90s, with the majority above 60

79 years of age (Fig S1A-D). Samples varied in viral load over >5 orders of magnitude as assessed by RT-
80 qPCR for the SARS-CoV-2 N1 gene or by read mapping of NP RNA to the SARS-CoV-2 genome, with a
81 strong correlation seen between PCR Ct value for the SARS-CoV-2 N1 gene and viral RNA reads by
82 RNA-Seq (r^2=0.8380, p<0.0001; Fig S1E).
83
84 Of reads mapping to the human genome, 1770 RNAs differed significantly between SARS-CoV-2+
85 patients and control subjects (Fig 1A). These included 1567 protein-coding genes, of which 1245 (79.4%)
86 were enriched and 322 reduced in patients relative to controls. The most significantly enriched genes in
87 the nasopharynx of SARS-CoV-2 patients were known interferon stimulated genes (ISGs), including three
88 NP ISG transcripts previously shown by our group to accurately identify patients with viral respiratory
89 infection, OASL, IFIT2, and CXCL10 (Fig 1A)(Landry and Foxman, 2018). Analysis of ingenuity pathways
90 and transcription factor binding sites associated with enriched transcripts demonstrated activation of
91 multiple pathways related to ISG induction in SARS-CoV-2 patients compared to controls, as well as
92 other pathways linked to innate immunity, leukocyte recruitment, and initiation of mucosal inflammatory
93 responses (Fig 1B-D).
94
95 Examination of gene expression across patient samples revealed several patterns (Fig 1E-G). First, the
96 45 most significantly enriched genes were all interferon stimulated genes, according to the Interferome
97 database (Rusinova et al., 2013). ISGs appeared to be co-regulated within individual patients, i.e.
98 patients with high expression of one ISG tended to have high expression of other ISGs (Fig 1E). This
99 was also demonstrated by analysis of the correlation between reads for different ISGs across samples
100 (Fig 1F). Second, ISG expression appeared to be loosely correlated with viral load, with those patients
101 with the highest viral load (Fig 1E, left) tending to have higher ISG expression than those with the lowest
102 viral loads (Fig 1E, right). However, while all SARS-CoV-2+ samples showed enrichment of ISG
103 expression compared to controls, direct comparison of DEGs in patient groups with distinct clinical

104 characteristics (sex, age, or outpatient/admitted status) showed no significant differences in ISG
105 expression.
106
107 Next, we measured the level of CXCL10 protein in the NP-swab associated viral transport medium using
108 ELISA. We previously showed that NP CXCL10 is detected in the viral transport medium during other
109 acute viral respiratory infections and correlates with expression of ISGs at the mRNA level (Landry and
110 Foxman, 2018). Consistently, we observed a significant positive correlation between NP CXCL10 protein
111 level with the NP mRNA level of Cxcl10 in SARS-CoV-2+ patient NP samples (Fig 1E, G). Together,
112 these results indicated that across subjects with diverse clinical presentations, SARS-CoV-2 induced a
113 robust interferon response in the nasopharynx and that the NP CXCL10 protein level correlated with ISG
114 expression at the RNA level.
115
116 **Relationship between SARS-CoV-2 viral load and NP host response in vivo**
117 Next, we sought to examine the host response during SARS-CoV-2 infection in a larger set of samples
118 from patients evaluated in our healthcare system in March and April of 2020 (n=140) (Fig 2 and Fig S2A,
119 B), to gain further insight into the relationship between viral replication, disease status, and host response
120 to infection. Based on our previous studies and our finding that NP CXCL10 protein level correlated with
121 ISG expression in SARS-CoV-2 positive samples (Fig 1), we used NP CXCL10 as an indicator of the
122 nasopharyngeal antiviral response. First, we examined NP CXCL10 level in SARS-CoV-2+ individuals
123 who were tested as outpatients and not admitted to the hospital, compared to those who were admitted.
124 Notably, we observed significantly higher NP CXCL10 levels in outpatients compared to admitted patients
125 (Fig 2A, p=0.0019). To understand the reason for this, we first examined patient age, since as a group,
126 admitted patients were significantly older than outpatients (16 years older on average, Fig S2C).
127 However, there was no correlation between age and CXCL10 level (Fig S2D). Next, we examined viral
128 load. We were initially surprised to find that admitted patients had significantly lower viral loads than
129 outpatients (Fig 2B). This suggested that the main factor driving CXCL10 level was viral load. Supporting

130 this idea, correlation analysis showed a significant positive correlation between NP CXCL10 level and
131 viral load by RT-qPCR (for all patients, r^2=0.2030, p<0.0001, Fig 2C). This correlation was also seen in
132 separate analyses of outpatients and admitted patients, with but no significant difference in the slope of
133 the CXCL10 vs viral load correlation between these groups, although there was a trend towards a higher
134 slope in outpatients (Fig 2C). We also observed no significant relationship between sex and NP CXCL10
135 or sex and viral load in this sample set (Fig S2 E,F).
136
137 Prior work on SARS-CoV-2 has shown that the nasopharyngeal viral load is highest in the first few days
138 of infection, and that the more severe symptoms of COVID-19 requiring hospitalization occur in the
139 second or third week of infection(Cevik, 2020). Therefore, we hypothesized that admitted patients may
140 have shown lower viral loads at the time of testing than outpatients because they presented later in
141 infection, after peak viral replication in the nasopharynx. Consistently, outpatients tended to report fewer
142 days of symptoms prior to testing compared to admitted patients, although this information was only
143 available for a subset of patients (about one-third, n=44; Fig 2D).
144
145 **Viral load and nasopharyngeal CXCL10 patterns in vivo over time**
146 To further evaluate the relationship between viral replication and the innate antiviral response in the
147 nasopharynx, we examined viral load and NP CXCL10 data in longitudinal samples. First, we examined
148 viral load from 29 inpatients from March 12 and April 30, 2020 for whom we had at ≥8 sequential tests
149 results for SARS-CoV-2 with at least the first sample tested using the CDC assay (our clinical laboratory
150 also had other testing platforms) (Fig 3, Table S1). At this time, most serial testing was aimed at patient
151 clearance for discharge. Consistently, the majority of patients (15/29) showed low viral loads (Ct N1>21)
152 which remained low throughout the time course. Another common pattern was high viral load in the first
153 sample (Ct N1<20) followed by a decline in viral load over time, similar to patterns reported in the literature
154 for patients who presented close to the start of symptomatic illness (7/29 patients, Fig 3A). These patients
155 showed high CXCL10 level in the sample with peak viral load and a decline in NP CXCL10 after the viral

156 load had decreased (Fig 3B). One patient had a consistently high NP viral loads for 20 days and did not
157 survive (not shown). Finally, a third pattern was seen in a several patients (6/29), in which the first sample
158 had a low viral load which subsequently increased to a high peak level (Ct N1<20), then decreased over
159 time (Fig 3). This pattern is consistent with patient presentation close to the start of infection. Two of
160 these patients had no symptoms of SARS-CoV-2 and the virus was detected incidentally on screening
161 during hospitalization for other reasons (Fig 3C,D, Table S1). One of these patients had an inconclusive
162 test and a positive test on the same day, 12 hours later (first test, N1 not detected, N2 Ct 38.4, second
163 test N1 Ct 34.6, N2 Ct 35.4), suggesting that this might have been the first day of infection for this patient
164 (L2, Fig 3C). The other four patients presented with acute symptoms including fever, and in some cases
165 cough and/or shortness of breath. NP CXCL10 in these patients was undetectable or low in the first
166 positive sample with low viral load, then rose with viral RNA, and then subsequently declined as viral load
167 declined. Together, the longitudinal data show a correlation with NP CXCL10 and viral load in individual
168 patients over time, similar to what we observed across 140 patients tested at a single time point (Fig. 2).
169 Notably, for patient L2, the only patient for whom three samples were available prior to peak viral load,
170 there appeared to be a delay between CXCL10 production relative to viral replication during the first few
171 days of infection, suggesting that initially viral replication outpaced the host innate immune response in
172 the nasopharynx.
173
174 **SARS-CoV-2 replication kinetics and ISG response early in infection**
175 To further evaluate the kinetics of SARS-CoV-2 replication and host response, we performed a time
176 course of SARS-CoV-2 infection using primary human airway epithelial cells grown at air-liquid interface,
177 which differentiate into organoids with beating cilia and mucus production, recapitulating the airway
178 mucosal surface in vivo. Cultures were inoculated with SARS-CoV-2 on the apical surface, washed after
179 1 hr, then incubated at 35°C to simulate the temperature of the upper respiratory tract and conducting
180 airways. Cultures were collected for RNA isolation and RT-qPCR at 1 hr (post-inoculation time point),
181 24hr, 48hr, 72hr, and 96hr and basolateral media was collected for CXCL10 ELISA. Reminiscent of what

182 we observed during SARS-CoV-2 infection in vivo (Fig 3D-I), viral load increased rapidly for the first three
183 days of infection, then plateaued between 72-96 hr (Fig 4A). ISGs were also induced, with ISG mRNA
184 levels and CXCL10 protein level in the basolateral medium increasing markedly from 72 to 96 hr (Fig 4B-
185 F). Notably, a very high level of CXCL10 protein was produced by infected epithelia (~4ng/ml by 96 hr),
186 consistent with the strong NP CXCL10 signal observed in the nasopharynx in vivo.
187

188 **Doubling time of SARS-CoV-2 in vitro and in vivo**

189 Viral replication in organoid cultures appeared to follow an exponential curve for the first 72hr of infection.
190 Therefore, we used curve-fitting to exponential growth to estimate the doubling time, which was 5.858 hr
191 (95% C.I. of 4.85-7.357 hr., based on 20 y-values, 5 per time point; Fig 4G). For patient L2, viral load
192 data from first three SARS-CoV-2+ time points also appeared to follow exponential growth, therefore we
193 used the same method to estimate the SARS-CoV-2 doubling time in vivo from this data, which was
194 6.454 hr (95% C.I. 4.261-13.30 hr based on 3 y-values, Fig 4H). For all other patients from whom viral
195 load increased in serial samples (Fig 3), we had only one sample prior to peak viral load. We asked what
196 the doubling times for SARS-CoV-2 would be in these samples if we assumed exponential replication
197 between the first and peak viral RNA values. The calculated doubling times across patients ranged from
198 3.048-6.509 hr for samples less than or equal to 5 days apart. For the two patients with a larger sampling
199 interval (L44, L12), calculated doubling times were 9.455 and 12.58 hr, although these calculations would
200 be expected to overestimate doubling time if the second sample was taken after viral replication had
201 plateaued or begun to decline. Together, the in vitro and in vivo results indicate that SARS-CoV-2
202 replicates exponentially during the first few days post-infection prior to the peak host anti-viral response,
203 with an average doubling time of approximately 6 hr.
204

205 **Effect of prior rhinovirus infection on ISG induction and SARS-CoV-2 replication**

206 One of the many physiological exposures that could potentially alter the local innate immune response
207 to SARS-CoV-2 in the upper airway mucosa is recent infection by other viruses. To model this situation,

208 we used organoid culture to examine the effects of prior exposure to rhinovirus, the most frequently
209 detected virus in the human upper respiratory tract, on subsequent SARS-CoV-2 infection (Fig 5A).
210 Based on previous studies, we expected that rhinovirus might curtail infection by inducing an epithelial
211 antiviral response, but also could potentially promote infection by increasing expression of SARS-CoV-2
212 entry receptors (Wu et al., 2020; Ziegler et al., 2020). Similar to previous observations, rhinovirus infection
213 (HRV-01A, MOI ~0.05) led to robust induction of interferon stimulated genes by day 3 post-infection (Fig
214 5B). We then evaluated whether rhinovirus infection altered the expression of ACE2, the SARS-CoV-2
215 entry receptor. ACE2 was originally reported to be an ISG, but a subsequent study reported that full-
216 length ACE2, which functions as an entry receptor, is not an ISG, and that a truncated form, dACE2, is
217 an ISG but is not a functional SARS-CoV-2 entry receptor (Onabajo et al., 2020; Ziegler et al., 2020).
218 Consistent with this finding, we observed that dACE-2 was significantly induced by rhinovirus infection
219 (~14-fold) and that, as expected for an ISG, induction was prevented by blocking activation of IRF3, a
220 transcription factor downstream of viral RNA sensors, using the inhibitor BX795 (Clark et al., 2009). In
221 contrast, full-length ACE2 expression was slightly but significantly increased by rhinovirus infection(~2-
222 fold) and this change was not abrogated by BX795, suggesting a different mechanism of induction (Fig
223 S3.) Rhinovirus infection had no effect on expression of TMPRSS2 (not shown).
224
225 Next, we evaluated SARS-CoV-2 replication and ISG induction following infection of airway epithelial
226 organoids, with or without prior rhinovirus infection. SARS-CoV-2 viral load increased exponentially in
227 infected cultures without prior RV infection, as observed previously (Fig 4), but showed essentially no
228 increase when cultures had been exposed to rhinovirus 3 days prior (Fig 5C). Evaluation of ISG
229 expression over the course of infection showed that at early time points of SARS-CoV-2 infection (24, 48
230 hr, and sometimes 72hr), ISGs were significantly more highly expressed in RV-preinfected cultures that
231 in cultures infected with SARS-CoV-2 without prior RV exposure (Fig 5D). This included several ISGs
232 which have been previously reported to limit coronavirus replication or for which polymorphisms are
233 linked to disease severity of SARS-CoV or SARS-CoV-2, including ISG15, BST2 (tetherin), and LY6E,

234 and OAS1-3 (Hamano et al., 2005; He et al., 2006; Ma et al., 2014; Martin-Sancho et al., 2020; Pairo-
235 Castineira et al., 2020; Pfaender et al., 2020; Taylor et al., 2015) (Fig 5D). Non-linear regression analysis
236 was consistent with exponential replication of SARS-CoV-2 from 24-72 hr post infection in mock-
237 pretreated cultures, in contrast to rhinovirus pre-infected cultures which supported essentially no
238 replication (Fig 5E).
239
240 To better understand the timing and breadth of the epithelial host response to rhinovirus that appeared
241 to limit SARS-CoV-2 replication, we evaluated ISG expression over time for five days post rhinovirus
242 infection and examined ISG expression and viral infection at the single cell level. Time course analysis
243 showed that following inoculation, rhinovirus replicated robustly, peaking at 24 hr post-infection, and then
244 declined significantly but was still detectable by RT-qPCR at day 5, a time point corresponding to 48 hr
245 post SARS-CoV-2 infection in the sequential infection experiment (FigS4A). ISG expression increased
246 and decreased in parallel with viral replication but was still significantly higher than in mock-treated cells
247 at day 5 post-rhinovirus infection(Fig S4B-E). Next, we performed single cell RNA sequencing to evaluate
248 the host ISG response in infected and bystander cells on day 5 post rhinovirus infection. At this time
249 point, rhinovirus viral RNA reads were detected in only 70 out of 4200 cells sequenced (Fig 5F). The
250 infected cells were predominantly ciliated cells but included all major cell types, consistent with the HRV-
251 01A entry receptor LDL-R being ubiquitously highly expressed throughout the culture (Fig S4F,G).
252 Although rhinovirus was only detected in a small subset of cells in infected cultures at day 5 (1.67%),
253 ISGs were elevated in all cells compared to mock-treated cultures (Fig 5F), demonstrating that rhinovirus
254 infection induces a robust bystander antiviral response in uninfected cells that lasts at least 5 days.
255
256 **Blocking ISG induction restores SARS-CoV-2 replication following rhinovirus infection**
257 Next, to test whether suppression of SARS-CoV-2 replication by rhinovirus was dependent upon the host
258 cell interferon response, we pre-treated cells with the signaling inhibitor BX795 18hr before rhinovirus
259 infection, which prevents interferon and ISG induction by rhinovirus(Fig 6A, B)(Clark et al., 2009; Wu et

260 al., 2020). There was no significant difference in SARS-CoV-2 viral load in RNA isolated from organoid
261 cultures at 72 hr for cultures with and without drug treatment, (Fig 6B). The effect of BX795 treatment
262 was much more striking in the setting of sequential rhinovirus-SARS-CoV-2 infection. As seen previously
263 (Fig 5), prior infection with rhinovirus suppressed SARS-CoV-2 replication by >1000-fold, but replication
264 was restored by BX795 pre-treatment (Fig 6C). These results indicate that IRF3 signaling is critical for
265 the inhibition of SARS-CoV-2 replication by prior rhinovirus infection, consistent with the effects of RV
266 pre-infection on ISG induction (Fig 5).
267
268 RV viral RNA was detected at much lower levels than SARS-CoV2 RNA at this time point (72hr post
269 SARS-CoV-2 infection, 6 days post-RV infection), and showed a slight reduction during SARS-CoV-2
270 coinfection without BX-795, but significantly higher levels during co-infection in the presence of BX-795.
271 This result indicates that the antiviral response limits rhinovirus replication in the setting of SARS-CoV-2
272 co-infection at this time point, and that both viruses achieve higher viral loads with inhibition of innate
273 antiviral signaling. In other words, in the presence of an intact antiviral response, viral load of both viruses
274 is reduced by co-infection, but if the host response is inhibited, the viral load of both viruses is higher
275 during co-infection. This experiment models viral co-infection in a host with an intact interferon response
276 (both viruses decrease during co-infection), compared to a host with a deficient interferon response
277 (equal or greater replication of both viruses during co-infection.)
278
279 **Blocking ISG induction enhances SARS-CoV-2 replication in a low MOI infection**
280 Next, we further probed the effect of BX-795 treatment on SARS-CoV-2 replication using a ten-fold lower
281 MOI (MOI ~0.05), conditions under which SARS-CoV-2 would potentially be more sensitive to
282 suppression by ISGs. Under these conditions, BX795 treatment led to a ~10-fold increase in intracellular
283 viral load and ~300-fold increase in virus shedding into the apical wash at 72 hr post infection. A trend
284 towards an increase (5-10x) was also seen at 96 hrs post-infection, although due to variability among
285 replicates this difference was not statistically significant (Fig 7A, B). Based on these results, we checked

286 the effect of BX795 on viral shedding into the apical wash in the MOI 0.5 infection (Fig 6) but in this case
287 results were similar to those observed in organoid cultures (not shown). Next, based on the increase in
288 viral RNA from 1hr to 72 hr during the low MOI infection, we estimated the effect of BX795 on the SARS-
289 CoV-2 doubling time in organoid culture. Assuming exponential growth between 1hr and 72 hr, the SARS-
290 CoV-2 doubling time without BX795 was 5.127 hr (95%C.I. 3.889 to 7.518 hrs), and with BX795 was
291 3.578 hr (95%C.I. 3.499 to 3.661). We then examined expression of ISGs that have been shown to limit
292 coronavirus replication and which have high basal expression in airway epithelial cultures including
293 IFITM3, ISG15, and BST2 (tetherin), thus could be particularly important for limiting a low MOI infection.
294 Induction of all of these ISGs was suppressed by BX795 pre-treatment (Fig 7D-F). For BST2 mRNA,
295 blocking ISG induction with BX795 revealed a decrease in BST2 mRNA below the baseline level during
296 SARS-CoV-2 infection, suggesting that SARS-CoV-2 may antagonize BST2 expression at the mRNA
297 level, in addition to other mechanisms whereby SARS-CoV-2 or SARS-CoV have been reported to
298 antagonize BST2 at the protein level (Martin-Sancho et al., 2020; Taylor et al., 2015). The effects of
299 BX795 on SARS-CoV-2 during low MOI infection indicate that the epithelial antiviral response induced
300 by SARS-CoV-2 does limit viral replication, albeit to a lesser extent than interference by rhinovirus.
301
302 Taken together, our results show that SARS-CoV-2 undergoes exponential replication at the start of
303 infection and induces ISG expression in vitro and in vivo, and that conditions which alter the initial ISG
304 expression level or rate of ISG induction, including prior infection by a different virus, can profoundly
305 impact SARS-CoV-2 replication.

306 **Discussion**

307 SARS-CoV-2 replication in the nasopharynx is known to peak during the first week of infection, but the
308 biological variables governing the rate and magnitude of viral amplification are not fully understood
309 (Cevik, 2020; He et al., 2020). Nasopharyngeal viral load early in infection correlates with likelihood of
310 transmitting the infection, and robust viral amplification in the respiratory tract is also likely a prerequisite,
311 although certainly not the only factor, for progression of COVID-19 disease. Here we present evidence
312 that during the first few days of SARS-CoV-2 infection, the airway interferon response plays a protective
313 role by curtailing viral replication in its initial target tissue: the airway epithelium. Specifically, our data
314 show that the extent of viral replication is determined by the magnitude and timing of the host interferon
315 response during a critical time window at the start of infection.

316

317 The interferon response is a potent mechanism of antiviral innate defense at mucosal surfaces and
318 effectively curtails replication of many viruses, most of which also antagonize this host response to some
319 degree in order to enable viral replication(Garcia-Sastre, 2017; Iwasaki, 2012). Viral recognition by innate
320 immune sensors within infected epithelial cells induces expression of type I and type III interferons and
321 interferon stimulated genes (ISGs), a diverse family of antiviral effectors, both directly, in infected cells,
322 and in neighboring cells through paracrine effects of secreted interferons(Odendall and Kagan, 2015;
323 Schneider et al., 2014). SARS-CoV-2 has been reported to induce interferons and ISGs in the airway
324 mucosa in vivo and in vitro (Mick et al., 2020; Mulay et al., 2020; Ravindra et al., 2020; Zhou et al., 2020).
325 Consistently, we observed robust ISG induction in all patients using RNA-Seq of nasopharyngeal RNA,
326 regardless of disease severity or other biological variables (Fig 1). However, there is also convincing
327 evidence that SARS-CoV-2 antagonizes the interferon response in infected cells through multiple
328 mechanisms(Banerjee et al., 2020a; Konno et al., 2020; Martin-Sancho et al., 2020; Xia et al., 2020).
329 Our observations with organoid culture (Fig 4), and in the one patient for whom we had multiple
330 longitudinal samples prior to peak viral load (patient L2, Fig 3A) show exponential viral replication at the
331 start of SARS-CoV-2 infection. ISGs are also induced, but it is unclear when this host response becomes

332 functionally effective. We found that in the first 72 hours of infection, prior to the peak host response,
333 blocking ISG induction had no effect in SARS-CoV infection at MOI 0.5 (Fig 6), but did increase viral
334 replication at ten-fold lower MOI (Fig 7; MOI 0.05). Together, these observations support a model in which
335 antagonism by SARS-CoV-2 attenuates but does not prevent the interferon response and thereby creates
336 a time window at the start of infection during which the virus can undergo exponential growth.
337
338 Due to the nature of exponential growth, a small change in biological variables affecting either the rate of
339 viral replication or the rate of development of an effective interferon response could have a profound
340 impact on viral amplification and peak viral load. For example, based on an average viral doubling time
341 estimated from our data of ~6 hr, a 24 hour delay in the development of an effective interferon response,
342 for example due to host deficiency in innate immune signaling, would lead to a 16-fold increase in peak
343 viral load. Thus, a peak viral load of 1000 infectious particles would become 16,000 infectious particles,
344 an upper airway viral load much more likely to lead to viral transmission or spread of the infection to the
345 lower respiratory tract. Likewise, if conditions or viral differences allowed the viral doubling time to
346 decrease by two hrs, from 6 hr to 4hr, this would lead to 16-fold greater viral amplification by 48 hr, and
347 64-fold greater amplification by 72hr, for the faster growing strain. The extent to which NP viral load
348 correlates with disease severity is still unclear, although several studies show an association (Huang et
349 al., 2020; Liu et al., 2020; Yilmaz et al., 2020; Zheng et al., 2020). However, there is strong evidence that
350 high NP viral load correlates with viral transmission, an issue that has come into focus recently due to
351 the emergence of SARS-CoV-2 strains that appear to have enhanced transmission, such as the B.1.1.7
352 strain emerging in the U.K.(Cevik, 2020; He et al., 2020; Prevention, 2021; Singanayagam et al., 2020)
353 Our study predicts biological features of the virus that could potentially underlie this greater
354 transmissibility, such as better antagonism of the host interferon response or faster doubling time, both
355 of which would be expected to increase NP viral load and therefore increase transmissibility.
356 Conversely, host factors that enhance interferon-mediated defenses could be impactful in reducing peak
357 viral load or even preventing infection altogether. One factor that is known to alter ISG expression in the

358 nasopharynx is recent viral infection. In this study, we focused on rhinovirus, the most frequent cause of
359 the common cold. Recent epidemiological studies have shown that this virus is much more prevalent in
360 the upper respiratory tract than previously appreciated (Foxman and Iwasaki, 2011; Jartti et al., 2008).
361 For example, in a recent year-round study, about one-third (34%) of all nasal samples from young children
362 (<5 yrs) were rhinovirus-positive, regardless of symptoms (Byington et al., 2015). Rhinoviruses and other
363 respiratory viruses have also been shown to induce ISGs in the nasopharynx in vivo, in both the presence
364 and absence of symptoms (Landry and Foxman, 2018; Wolsk et al., 2016; Yahya et al., 2017; Yu et al.,
365 2019). Thus, rhinovirus fits the characteristics of a common environmental factor that could impact ISG
366 expression in the respiratory tract.
367
368 Our studies using sequential infection in an airway epithelial organoid model show that prior rhinovirus
369 infection blocks replication of SARS-CoV-2 that this protection is dependent upon ISG induction.
370 Furthermore, using time course studies and single cell analysis of organoid cultures, we found that a
371 significant bystander interferon response can be detected in cells throughout the epithelium for at least 5
372 days post-rhinovirus infection, even though viral replication peaks at 24 hr and few infected cells are
373 detected at this time point (Fig 5, Fig S4). This finding is consistent with recent work from our group and
374 others showing that the host interferon response triggered by one respiratory virus can block infection by
375 another (Essaidi-Laziosi et al., 2020; Wu et al., 2020). Viral interference seen during sequential influenza
376 virus infections was in fact the basis for the original discovery and naming of interferons in 1957, but only
377 recently has this idea been explored in depth with regards to human respiratory viral infections, triggered
378 in part by epidemiological data suggesting interference among RNA respiratory viruses(Greer et al.,
379 2009; Isaacs and Lindenmann, 1957; Karppinen et al., 2016; Nickbakhsh et al., 2019; Schultz-Cherry,
380 2015). ISG induction by an unrelated virus may be particularly effective against a virus like SARS-CoV-
381 2, since it would pre-empt many of the mechanisms SARS-CoV-2 has in place to antagonize interferon
382 and ISG induction in response to its own replication, including specific targeting of ISGs effective in
383 blocking the coronavirus life cycle such as BST2 (Martin-Sancho et al., 2020; Taylor et al., 2015).

384 The concept of viral interference based on the host interferon response assumes a host with intact innate
385 immune defenses, which may not always be the case. In our experimental model, there was a profound
386 difference in the outcome of rhinovirus-SARS-CoV-2 co-infection in the presence and absence of an
387 intact host cell interferon response (Fig 6). With an intact host response, viral loads of both viruses
388 decreased, but when the interferon response was blocked, viral loads of both viruses were equal to or
389 higher than in single infections (Fig 6.) This result illustrates that the expected outcome of a viral co-
390 infection is not one-size-fits-all: it is likely to be profoundly dependent upon host innate immune status.
391 Many host factors ranging from genetic polymorphisms to transient environmental conditions in the
392 airway (e.g. temperature, humidity) can attenuate interferon responses and promote replication of
393 respiratory viruses, and would likewise be expected to reduce the interferon-mediated protective effects
394 of viral co-infection (Asgari et al., 2017; Foxman et al., 2015; Kudo et al., 2019; Lamborn et al., 2017;
395 Mihaylova et al., 2018; Zhang et al., 2020). Also, interference requires closely spaced virus co-exposures,
396 which may be less frequent at certain times of the year, or during the use of pandemic mitigation
397 measures. Low rates of influenza during 2020 in the southern hemisphere indicate that the public health
398 measures put in place to slow the spread of SARS-CoV-2 also suppressed circulation of other respiratory
399 viruses, although there is some evidence that rhinoviruses have continued to circulate(Olsen et al., 2020;
400 Poole et al., 2020). Viral interference may become a more important consideration for understanding
401 susceptibly to COVID-19 and other viral pathogens as society reopens.
402
403 There are several important caveats to our study. First, our data indicate a relatively limited effect of the
404 SARS-CoV-2-induced interferon response on initial viral replication when it is the only virus present, at
405 least at high MOI (Fig 6). However, the recruitment of cells of the immune system to the respiratory tract,
406 as indicated by our RNAseq data (Fig 1), could considerably amplify ISG induction in vivo. Recent work
407 showing that interferon deficiencies are linked to severe COVID-19 indicates the importance of interferon-
408 mediated defense against this virus in vivo (Bastard et al., 2020; Pairo-Castineira et al., 2020; Zhang et
409 al., 2020). Second, in vivo virus-host-virus interactions could be more complicated than those seen in

410 organoid culture; for example, if a viral infection results in residual lung damage this could exacerbate
411 rather than protect against a subsequent viral respiratory illness. Studying virus-host-virus interactions in
412 vivo will be an important future direction of this study. For assessing viral interference, it will be critical
413 not only to look at co-occurrence or sequential occurrence of viral infections, but also to measure the
414 antiviral response in vivo. For example, symptomatic upper respiratory tract infections induce greater
415 ISG responses than asymptomatic, and the latter may not cause significant interference(Yahya et al.,
416 2017). Such studies will be facilitated by increasing development of nasopharyngeal swab-based
417 methods to assess the airway host immune response, as presented here and in the recent
418 literature(Landry and Foxman, 2018; Mick et al., 2020; Wolsk et al., 2016; Yu et al., 2019).
419
420 In sum, our results demonstrate an important role for the interferon-mediated defenses in curtailing
421 SARS-CoV-2 replication at the start of infection and compel further studies of how the changing
422 conditions present in the upper respiratory tract, including recent infection by other viruses, can modulate
423 host antiviral defenses and alter SARS-CoV-2 infection and transmission.

424 **Acknowledgements**

425 We would like to thank Craig Wilen and Wilen lab members for valuable help and advice, and for providing
426 SARS-CoV-2 virus stock. We thank Maureen Owen, Robin Garner, Greta Edelman, the entire staff of
427 the Yale New Haven Hospital Clinical Virology laboratory, and Amy Likens for their dedicated assistance.
428 We also thank Bryan Pasqualucci and Christopher Castaldi at the Yale Center for Genomic Analysis.
429 Funding was provided by Fast Grants (Emergent Ventures, Mercatus Institute, George Mason University)
430 to E.F.F., the Yale Department of Laboratory Medicine and COVID-19 Dean's Fund (E.F.F.), the China
431 Scholarship Council-Yale World Scholars Fellowship (B.W.), the Gruber Foundation Fellowship (T.W.),
432 and the NIH (T32AI007019, T.W.).

433

434 **Author Contributions**

435 Conceptualization E.F.F.; Methodology, N.R.C., T.W., V.T.M., B.W., D.Z., M.L.L., and E.F.F.;
436 Investigation N.R.C., T.W., V.T.M., B.W., and E.F.F.; Formal analysis B.W., D.Z., and G.W.; Resources,
437 M.L.L.; Writing – Original Draft, E.F.F.; Writing – Review & Editing, N.R.C., T.W., V.T.M., B.W.,D.Z., G.W.,
438 M.L.L., E.F.F.; Funding Acquisition, E.F.F.

439

440 **Declaration of Interests**

441 Dr. Foxman is an inventor on a pending patent application WO2019/217296 A1 and Dr. Foxman and Dr.
442 Landry are inventors on pending patent application WO2018/071498 Al. The other authors declare no
443 competing interests.

Methods details

RESOURCE AVAILABILITY

Lead Contact

Further information and requests may be directed to, and will be fulfilled by the lead contact Ellen F. Foxman, ellen.foxman@yale.edu

Materials availability

This study did not generate new reagents.

Data and Code Availability

Nasopharyngeal transcriptome data and single cell RNA sequencing data will be publicly available in the GEO database at the time of publication.

EXPERIMENTAL MODEL AND SUBJECT DETAILS

Ethics statement

The use of clinical samples and data in this study was approved by the Yale Human Research Protection Program Institutional Review Board (Protocol ID #200002765). Procedures for testing residual clinical samples and recording linked patient data, followed by sample and data de-identification, were evaluated and the requirement for specific patient consent was waived. In vitro experiments used primary human cells obtained from Lonza Bioscience (Walkersville, Maryland, U.S.A.). Lonza guarantees that all tissue utilized for human cell products is ethically obtained with donor informed consent in accordance with processes approved by an Institutional Review Board or comparable independent review body.

Clinical samples

We used viral residual nasopharyngeal (NP) samples remaining after clinical testing for CXCL10 measurements and transcriptome analysis. Swab-associated viral transport medium was stored at -80

470 °C following clinical testing and thawed just prior to ELISA assay or RNA isolation for RNA-Seq. Clinical
471 information including age, sex, virology results, and specific features of clinical course including
472 presenting symptoms, hospital admission and length of stay, was extracted from the electronic medical
473 record and recorded, after which samples were assigned a study code and de-identified. In the clinical
474 laboratory, SARS-CoV-2 was detected in most samples using an EUA-approved TaqMan assay detecting
475 the CDC targets N1, N2, and RNAseP (Prevention, 2020). In some longitudinal samples, SARS-CoV-2
476 was diagnosed with the commercial Cepheid assay (reference); in this case, RT-qPCR for the CDC N1
477 gene was repeated using RT-qPCR TaqMan assay for the CDC N1 gene as described previously (Cat
478 no: 10006600, Integrated DNA Technologies, IA)(Vogels et al., 2020).
479
480 *Primary human bronchial epithelial cells.*
481 Primary human bronchial epithelial cells from healthy adult donors were obtained commercially (Lonza,
482 Walkersville, MD, USA) and cultured at air-liquid interface according to manufacturer's instructions using
483 reduced hydrocortisone (Stem Cell Technologies, Vancouver, Canada). Cells were allowed to
484 differentiate for four weeks by which time they displayed beating cilia and mucus production.
485
486 *Viruses*
487 Rhinovirus 1A (HRV-01A; ATCC VR-481) was amplified in H1-HeLa cells (ATCC CRL-1985) and titer
488 was determined by plaque assay as reported previously (Foxman et al., 2015). SARS-CoV-2 (BEI
489 resources, USA-WA1/2020) was generously provided by the Wilen lab. Virus was cultured on Vero E6
490 cells and titer was determined by plaque assay as described previously (Ravindra et al., 2020).
491
492 *RNA isolation from clinical samples*
493 At the time of accessioning, the residual viral transport medium from clinical samples was stored at -80C.
494 Upon thawing, RNA was isolated from 140µl of transport medium using the Qiagen Viral RNA isolation

495 kit per manufacturer's instructions (Ref: 52904, Qiagen, Germany) and one aliquot was reserved for
496 ELISA.

497 *Library preparation and RNA Sequencing*

498 RNA samples were quantified and checked for quality using the Agilent 2100 Bioanalyzer Pico RNA
499 Assay. Library preparation was performed using Kapa Biosystem's KAPA HyperPrep Kit with RiboErase
500 (HMR) in which samples were normalized with a total RNA input of 25ng. Libraries were amplified using
501 15 PCR cycles. Libraries were validated using Agilent TapeStation 4200 D1000 assay and quantified
502 using the KAPA Library Quantification Kit for Illumina® Platforms kit. Libraries were diluted to 1.3nM and
503 pooled at 1.25% each of an Illumina NovaSeq 6000 S4 flowcell using the XP workflow to generate 25M
504 read pairs / sample.

505

506 *RNA-Seq data analysis*

507 Low quality reads were trimmed and adaptor contamination was removed using Trim Galore (v0.5.0,
508 https://www.bioinformatics.babraham.ac.uk/projects/trim_galore/). Trimmed reads were mapped to the
509 human reference genome (hg38) using HISAT2 (v2.1.0)(Kim et al., 2019). Gene expression levels were
510 quantified using StringTie (v1.3.3b) with gene models (v27) from the GENCODE project(Pertea et al.,
511 2015). Differentially expressed genes (adjusted p value < 0.05, fold change cutoff = 2) were identified
512 using DESeq2 (v 1.22.1) (Love et al., 2014). To avoid the unexpected outlier replacement for sex-linked
513 genes, we turned off the outlier replacement option in the male vs. female comparison by setting
514 minReplicatesForReplace=Inf for the DESeq() function in the DESeq2 package.

515

516 *Visualization of RNA-Seq data.* Protein coding genes differentially expressed in SARS-CoV-2+ vs.
517 negative control were visualized on a volcano plot, with an x-axis cutoff l $\log_2$FC cutoff l =10. All
518 differentially expressed RNAs are included in Table S1 (n=1770). Significantly differentially expressed
519 transcripts were defined as those with $\log_2$FC>1 and adjusted p value<0.05. Heatmap shows gene
520 expression levels of top 45 most significant DEGs using min-to-max scaling of normalized read counts.

521 Pathway analysis was performed using Ingenuity Pathway Analysis (version 01-16). Transcription factor
522 motif enrichment analysis was performed using Cytoscape (version 3.8.1) with the iRegulon plug-in
523 ((version 1.3)(Janky et al., 2014).
524
525 *In vitro infections*
526 We infected primary human bronchial epithelial cells differentiated at air-liquid interface with HRV-01A,
527 SARS-CoV-2, or both. For SARS-CoV-2, high MOI infection was MOI 0.5 and low MOI infection was MOI
528 0.05. For HRV-01A, MOI 0.1 was used, as this was the minimum viral inoculum that reproducibly led to
529 robust HRV-01A viral replication in ALI cultures based on prior studies.
530
531 To evaluate the effect of RV on subsequent infection with SARS-CoV-2, we infected with each virus
532 individually or sequentially and examined the time course of viral amplification and ISG induction. To
533 formally test whether prior exposure to RV inhibits SARS-CoV-2 replication through activation of the host
534 cell interferon response, we performed sequential infection studies in the presence of BX795.
535
536 *RT-qPCR*
537 For RT-qPCR, RNA was isolated from each well of differentiated epithelial cells using the QIAGEN
538 RNeasy kit by incubating each 24-well insert with 350 μl lysis buffer at room temperature for 5 minutes,
539 followed by RNA isolation and cDNA synthesis using iScript cDNA synthesis kit (BioRad). To quantify
540 viral RNA and mRNA levels for interferon stimulated genes and the housekeeping gene HPRT, qPCR
541 was performed using SYBR green iTaq universal (BioRad) per manufacturer's instructions. Viral RNA
542 was quantified using primers to the RV genome. Viral RNA per ng total RNA is graphed as fold change
543 from the limit of detection (40 cycles of PCR) as 2^{40-Ct}. ISG mRNA levels are graphed as fold change from
544 mock-treated cells or are presented relative to the level of mRNA for the housekeeping gene HRPT (2^{-}
545 $^{\Delta\Delta CT}$). RT-qPCR for SARS-CoV-2 within cultures was performed using the previously-described TaqMan

546 assay for the CDC N1 gene with primers and probes provided by IDT (Cat no: 10006600, Integrated DNA
547 Technologies, IA). RT-qPCR for SARS-CoV-2 in apical was performed using a combined reverse
548 transcriptase and qPCR reaction using the Luna Universal Probe One-Step RT-qPCR Kit (New England
549 Biolabs, MA)
550
551 The following primers were used for RT-qPCR with SYBR green:
552 HPRT (F-TGGTCAGGCAGTATAATCCAAAG; R- TTTCAAATCCAACAAAGTCTGGC)
553 ISG15 (F-CATCTTTGCCAGTACAGGAGC; R-GGGACACCTGGAATTCGTTG)
554 RSAD2 (F-TCGCTATCTCCTGTGACAGC;R-CACCACCTCCTCAGCTTTTG)
555 MX1 (F-AGAGAAGGTGAGAAGCTGATCC;R-TTCTTCCAGCTCCTTCTCTCTG)
556 IFITM3 (F-ATCGTCATCCCAGTGCTGAT;R-ATGGAAGTTGGAGTACGTGG)
557 IFIT2 (F-CCTCAAAGGGCAAAACGAGG; R-CTGATTTCTGCCTGGTCAGC)
558 CXCL10 (F-CCTGCAAGCCAATTTTGTCC; R-ATGGCCTTCGATTCTGGATTC
559 LY6E (F-GCATTGGGAATCTCGTGACA; R-ATGGAAGCCACACCAACATT)
560 BST2 (F-CACACTGTGATGGCCCTAAT; R-TGTAGTGATCTCTCCCTCAAGC)
561 IFITM3 (F-ATCGTCATCCCAGTGCTGAT; R-ATGGAAGTTGGAGTACGTGG)
562 OAS1 (F-GCTCCTACCCTGTGTGTGTGT; R-TGGTGAGAGGACTGAGGAAGA)
563 OAS3 (F-GAAAACTGTCAAGGGAGGCTC; OAS3 R-CCCTCTGGTCCACATAGCTC)
564 HRV-01A (F- CAGGCCAAATTAAAGTCAATAAGC; R- AGGCTGAAGTTTGGTTTTGC)
565
566 ***Quantification and statistical analysis, RT-qPCR data***
567 GraphPad Prism (version 9.0.0) was used for data analysis. Data are shown as mean +/- S.E.M.
568 Statistical significance of differences between conditions was determined by t tests (two-tailed). Linear
569 regression analysis was used to determine association between clinical parameters, such as viral load
570 and NP CXCL10 in clinical samples and to test the null hypothesis that the slope of the association was
571 significantly different from zero. Non-linear regression analysis was used to fit viral growth to an

572 exponential curve (exponential growth with log(population)) to determine virus doubling times and to test
573 the null hypothesis that one curve fit both data sets for SARS-CoV-2 growth curve with and without
574 rhinovirus pre-infection. $p<0.05$ was considered statistically significant.
575
576 ***ELISA***
577 CXCL10 levels in cell-free residual nasopharyngeal swab samples or tissue culture supernatants was
578 quantified using a solid phase sandwich enzyme linked immunosorbent assay (ELISA) (Cat no: DY266,
579 R&D systems, MN). Briefly, frozen viral transport medium from residual nasopharyngeal swab samples
580 or basolateral medium from organoid cultures was thawed on ice and centrifuged to remove cell debris.
581 ELISA was performed according to the manufacturer's instructions.
582
583 **Single cell RNA-Seq of ALI organoid cultures**
584 *Library preparation and sequencing*
585 Organoid cultures were digested with trypsin/EDTA to form a single cell suspension. The 10X genomics
586 Single Cell 3' Protocol was used to produce Illumina-ready sequencing libraries with standard Illumina
587 paired-end constructs, according to the manufacturer's instructions.
588
589 *Analysis of scRNA-Seq data*
590 All downstream analyses were implemented using R version 3.6.3 and the package Seurat v3.1.4(Stuart
591 et al., 2019). The gene expression matrix mock and RV1A infected sample were first individually analyzed
592 in this procedure: Genes expressed in less than 3 cells and cells expressing less than 200 genes were
593 discarded. A distribution histogram of UMI count in all cells was made and cells with less than 8000 UMI
594 counts were discarded. This resulted in a matrix of 21086 genes expressing in 4511 cells in mock sample,
595 and a matrix of 21195 genes expressing in 4200 cells in RV1A infected sample. The raw counts were
596 normalized using the Seurat function NormalizeData with normalization.method = "LogNormalize" and
597 scale.facto = 10000. All genes are scaled using Seurat function ScaleData with default parameters.

598 Variable features were determined using method "vst". A total of top 2000 variable features were used
599 for principal component analysis (PCA). Graph based clustering was performed individually on mock and
600 RV1A infected sample. The KNN graph was built by FindNeighbors function with first 20 principal
601 components and k.param = 10. Louvain clustering was done using FindCluster function with resolution =
602 0.8 for both samples. Clusters were separately annotated in the mock and RV1A infected sample using
603 the following markers of the major cell groups in the airway epithelium: Basal Cycling (MKI67,
604 HIST1H4C), Basal (KRT14, KRT15, KRT5), Hillock (SPINK5, KRT13), Secretory (SCGB1A1, BPIFA1,
605 LYPD2), Ciliated (CAPS, PIFO, MORN2), Ionocyte (FOXI1) and PNEC(pulmonary neuroendocrine cells,
606 markers include AZGP1, AVIL)(Plasschaert et al., 2018). Each cluster found by clustering was assigned
607 to one of the above seven major groups. A group of developing ciliated cells with marker CCNO was
608 found in the mock sample and was merged into the ciliated cell cluster. After cluster annotation, mock
609 and infected samples were merged together to produce tSNE maps and make comparisons. Both
610 samples used same normalization method and the gene expression level was re-scaled. Dimensionality
611 reduction was performed by latent semantic analysis using Seurat function RunLSI with the first 50
612 singular values. The tSNE maps were then produced with the first 50 dimensions and perplexity 30. The
613 color coding of tSNE plots used cell type, sample source, viral read per cell and expression levels of
614 genes of interest.

615 **KEY RESOURCES TABLE**

REAGENT or RESOURCE	SOURCE	IDENTIFIER
Bacterial and Virus Strains		
HRV-01A	ATCC	ATCC VR-481
SARS-CoV-2	BEI resources	USA-WA1/2020
Biological Samples		
Residual nasopharyngeal samples from clinical testing	Yale-New Haven Hospital	
Chemicals, Peptides, and Recombinant Proteins		
BX795	Millipore Sigma	SML0694
Critical Commercial Assays		
iTaq Universal SYBR Green Supermix	BioRad	172-5125
iScript cDNA synthesis kit	BioRad	170-8891BUN
Primer-probe assay for SARS-CoV-2 (N1 gene)	IDT resources	10006600
Luna Universal Probe One-Step RT-qPCR Kit	New England Biolabs	E3006L
QIAamp Viral RNA isolation kit	QIAGEN	52904
QIAGEN RNeasy RNA isolation kit	QIAGEN	74106
Human CXCL10/IP-10 Duoset ELISA kit	R& D systems	DY266
Deposited Data		
Nasopharyngeal transcriptome data – deposited in GEO		
Single cell RNA-Seq data – deposited in GEO		
Experimental Models: Cell Lines		
NHBE-Bronchial Epi Cells for ALI	Lonza Walkersville Inc.	CC-2540S
H1 HeLa cells	ATCC	ATCC CRL-1958
Vero E6 cells	ATCC	ATCC CRL-1586
Oligonucleotides		
Primer sequences provided in Methods details		
Software and Algorithms		
R	www.r-project.org	SCR_001905
Seurat	satijalab.org/seurat/	RRID:SCR_016341
Prism v. 9.0.0 for MacOS	GraphPad	RRID:SCR_005375
Excel v. 16.43	Microsoft	RRID:SCR_016137
Ingenuity Pathway Analysis	QIAGEN	RRID: SCR_008653
Cytoscape	Open source	RRID: SCR_003032

616

References

Asgari, S., Schlapbach, L.J., Anchisi, S., Hammer, C., Bartha, I., Junier, T., Mottet-Osman, G., Posfay-Barbe, K.M., Longchamp, D., Stocker, M.*, et al.* (2017). Severe viral respiratory infections in children with IFIH1 loss-of-function mutations. Proceedings of the National Academy of Sciences of the United States of America *114*, 8342-8347.

Banerjee, A.K., Blanco, M.R., Bruce, E.A., Honson, D.D., Chen, L.M., Chow, A., Bhat, P., Ollikainen, N., Quinodoz, S.A., Loney, C.*, et al.* (2020a). SARS-CoV-2 Disrupts Splicing, Translation, and Protein Trafficking to Suppress Host Defenses. Cell.

Banerjee, A.K., Blanco, M.R., Bruce, E.A., Honson, D.D., Chen, L.M., Chow, A., Bhat, P., Ollikainen, N., Quinodoz, S.A., Loney, C.*, et al.* (2020b). SARS-CoV-2 Disrupts Splicing, Translation, and Protein Trafficking to Suppress Host Defenses. Cell *183*, 1325-1339 e1321.

Bastard, P., Rosen, L.B., Zhang, Q., Michailidis, E., Hoffmann, H.H., Zhang, Y., Dorgham, K., Philippot, Q., Rosain, J., Beziat, V.*, et al.* (2020). Autoantibodies against type I IFNs in patients with life-threatening COVID-19. Science *370*, eabd4585.

Blanco-Melo, D., Nilsson-Payant, B.E., Liu, W.C., Uhl, S., Hoagland, D., Moller, R., Jordan, T.X., Oishi, K., Panis, M., Sachs, D.*, et al.* (2020). Imbalanced Host Response to SARS-CoV-2 Drives Development of COVID-19. Cell *181*, 1036-1045 e1039.

Byington, C.L., Ampofo, K., Stockmann, C., Adler, F.R., Herbener, A., Miller, T., Sheng, X., Blaschke, A.J., Crisp, R., and Pavia, A.T. (2015). Community Surveillance of Respiratory Viruses Among Families in the Utah Better Identification of Germs-Longitudinal Viral Epidemiology (BIG-LoVE) Study. Clinical infectious diseases : an official publication of the Infectious Diseases Society of America *61*, 1217-1224.

Cevik, M., Tate, M., Lloyd, O., Maraolo, A.E., Scahfers, J., and A. Ho (2020). SARS-CoV-2, SARS-CoV, and MERS-CoV viral load dynamics, duration of viral shedding, and infectiousness: a systematic review and meta-analysis. The Lancet Microbe *20*, 30172-30175.

Clark, K., Plater, L., Peggie, M., and Cohen, P. (2009). Use of the pharmacological inhibitor BX795 to study the regulation and physiological roles of TBK1 and IkappaB kinase epsilon: a distinct upstream kinase mediates Ser-172 phosphorylation and activation. J Biol Chem *284*, 14136-14146.

Dong, E., Du, H, L Gardner (2020). An interactive web-based dashboard to track COVID-19 in real time. ; published online Feb 19.

Essaidi-Laziosi, M., Geiser, J., Huang, S., Constant, S., Kaiser, L., and Tapparel, C. (2020). Interferon-Dependent and Respiratory Virus-Specific Interference in Dual Infections of Airway Epithelia. Sci Rep *10*, 10246.

Feld, J.J., et al (2020). Peginterferon-lambda for the treatment of COVID-19 in outpatients. MedRxiv, https://doiorg/101101/2020110920228098.

Foxman, E.F., and Iwasaki, A. (2011). Genome-virome interactions: examining the role of common viral infections in complex disease. Nature reviews Microbiology *9*, 254-264.

Foxman, E.F., Storer, J.A., Fitzgerald, M.E., Wasik, B.R., Hou, L., Zhao, H., Turner, P.E., Pyle, A.M., and Iwasaki, A. (2015). Temperature-dependent innate defense against the common cold virus limits viral replication at warm temperature in mouse airway cells. Proceedings of the National Academy of Sciences of the United States of America *112*, 827-832.

Garcia-Sastre, A. (2017). Ten Strategies of Interferon Evasion by Viruses. Cell Host Microbe *22*, 176-184.

Greer, R.M., McErlean, P., Arden, K.E., Faux, C.E., Nitsche, A., Lambert, S.B., Nissen, M.D., Sloots, T.P., and Mackay, I.M. (2009). Do rhinoviruses reduce the probability of viral co-detection during acute respiratory tract infections? J Clin Virol *45*, 10-15.

Hamano, E., Hijikata, M., Itoyama, S., Quy, T., Phi, N.C., Long, H.T., Ha, L.D., Ban, V.V., Matsushita, I., Yanai, H.*, et al.* (2005). Polymorphisms of interferon-inducible genes OAS-1 and MxA associated with SARS in the Vietnamese population. Biochem Biophys Res Commun *329*, 1234-1239.

He, J., Feng, D., de Vlas, S.J., Wang, H., Fontanet, A., Zhang, P., Plancoulaine, S., Tang, F., Zhan, L., Yang, H., *et al.* (2006). Association of SARS susceptibility with single nucleic acid polymorphisms of OAS1 and MxA genes: a case-control study. BMC Infect Dis *6*, 106.

He, X., Lau, E.H.Y., Wu, P., Deng, X., Wang, J., Hao, X., Lau, Y.C., Wong, J.Y., Guan, Y., Tan, X., *et al.* (2020). Temporal dynamics in viral shedding and transmissibility of COVID-19. Nat Med *26*, 672-675.

Huang, J.T., Ran, R.X., Lv, Z.H., Feng, L.N., Ran, C.Y., Tong, Y.Q., Li, D., Su, H.W., Zhu, C.L., Qiu, S.L., *et al.* (2020). Chronological Changes of Viral Shedding in Adult Inpatients With COVID-19 in Wuhan, China. Clinical infectious diseases : an official publication of the Infectious Diseases Society of America *71*, 2158-2166.

Isaacs, A., and Lindenmann, J. (1957). Virus interference. I. The interferon. Proc R Soc Lond B Biol Sci *147*, 258-267.

Iwasaki, A. (2012). A virological view of innate immune recognition. Annu Rev Microbiol *66*, 177-196.

Janky, R., Verfaillie, A., Imrichova, H., Van de Sande, B., Standaert, L., Christiaens, V., Hulselmans, G., Herten, K., Naval Sanchez, M., Potier, D., *et al.* (2014). iRegulon: from a gene list to a gene regulatory network using large motif and track collections. PLoS Comput Biol *10*, e1003731.

Jartti, T., Jartti, L., Peltola, V., Waris, M., and Ruuskanen, O. (2008). Identification of respiratory viruses in asymptomatic subjects: asymptomatic respiratory viral infections. Pediatr Infect Dis J *27*, 1103-1107.

Karppinen, S., Toivonen, L., Schuez-Havupalo, L., Waris, M., and Peltola, V. (2016). Interference between respiratory syncytial virus and rhinovirus in respiratory tract infections in children. Clin Microbiol Infect *22*, 208 e201-208 e206.

Kim, D., Paggi, J.M., Park, C., Bennett, C., and Salzberg, S.L. (2019). Graph-based genome alignment and genotyping with HISAT2 and HISAT-genotype. Nat Biotechnol *37*, 907-915.

Konno, Y., Kimura, I., Uriu, K., Fukushi, M., Irie, T., Koyanagi, Y., Sauter, D., Gifford, R.J., Consortium, U.-C., Nakagawa, S., *et al.* (2020). SARS-CoV-2 ORF3b Is a Potent Interferon Antagonist Whose Activity Is Increased by a Naturally Occurring Elongation Variant. Cell Rep *32*, 108185.

Kudo, E., Song, E., Yockey, L.J., Rakib, T., Wong, P.W., Homer, R.J., and Iwasaki, A. (2019). Low ambient humidity impairs barrier function and innate resistance against influenza infection. Proceedings of the National Academy of Sciences of the United States of America *116*, 10905-10910.

Lamborn, I.T., Jing, H., Zhang, Y., Drutman, S.B., Abbott, J.K., Munir, S., Bade, S., Murdock, H.M., Santos, C.P., Brock, L.G., *et al.* (2017). Recurrent rhinovirus infections in a child with inherited MDA5 deficiency. J Exp Med *214*, 1949-1972.

Landry, M.L., and Foxman, E.F. (2018). Antiviral Response in the Nasopharynx Identifies Patients With Respiratory Virus Infection. The Journal of infectious diseases *217*, 897-905.

Lee, J.S., and Shin, E.C. (2020). The type I interferon response in COVID-19: implications for treatment. Nat Rev Immunol *20*, 585-586.

Liu, Y., Yan, L.M., Wan, L., Xiang, T.X., Le, A., Liu, J.M., Peiris, M., Poon, L.L.M., and Zhang, W. (2020). Viral dynamics in mild and severe cases of COVID-19. Lancet Infect Dis *20*, 656-657.

Lokugamage, K.G., Hage, A., de Vries, M., Valero-Jimenez, A.M., Schindewolf, C., Dittmann, M., Rajsbaum, R., and Menachery, V.D. (2020). Type I Interferon Susceptibility Distinguishes SARS-CoV-2 from SARS-CoV. J Virol *94*, e01410-01420.

Love, M.I., Huber, W., and Anders, S. (2014). Moderated estimation of fold change and dispersion for RNA-seq data with DESeq2. Genome Biol *15*, 550.

Lucas, C., Wong, P., Klein, J., Castro, T.B.R., Silva, J., Sundaram, M., Ellingson, M.K., Mao, T., Oh, J.E., Israelow, B., *et al.* (2020). Longitudinal analyses reveal immunological misfiring in severe COVID-19. Nature *584*, 463-469.

Ma, X.Z., Bartczak, A., Zhang, J., He, W., Shalev, I., Smil, D., Chen, L., Phillips, J., Feld, J.J., Selzner, N., *et al.* (2014). Protein interferon-stimulated gene 15 conjugation delays but does not overcome coronavirus proliferation in a model of fulminant hepatitis. J Virol *88*, 6195-6204.

Martin-Sancho, L., Lewinski, M.K., Pache, L., Stoneham, C.A., Yin, X., Pratt, D., Churas, C., Rosenthal, S.B., Liu, S., De Jesus, P.D., *et al.* (2020). Functional Landscape of SARS-CoV-2 Cellular Restriction. bioRxiv.

Mick, E., Kamm, J., Pisco, A.O., Ratnasiri, K., Babik, J.M., Castaneda, G., DeRisi, J.L., Detweiler, A.M., Hao, S.L., Kangelaris, K.N., *et al.* (2020). Upper airway gene expression reveals suppressed immune responses to SARS-CoV-2 compared with other respiratory viruses. Nat Commun *11*, 5854.

Mihaylova, V.T., Kong, Y., Fedorova, O., Sharma, L., Dela Cruz, C.S., Pyle, A.M., Iwasaki, A., and Foxman, E.F. (2018). Regional Differences in Airway Epithelial Cells Reveal Tradeoff between Defense against Oxidative Stress and Defense against Rhinovirus. Cell Rep *24*, 3000-3007 e3003.

Monk, P.D., Marsden, R.J., Tear, V.J., Brookes, J., Batten, T.N., Mankowski, M., Gabbay, F.J., , Davies, D.E., Holgate, S.T., Ho, L., Clark, T., Djukanovic, R., Wilkinson, T.M.A. (2020). Safety and efficacy of inhaled nebulised interferon beta-1a (SNG001) for treatment of SARS-CoV-2 infection: a randomised, double-blind, placebo-controlled, phase 2 trial. Lancet Respiratory Medicine *20*, 30511-30517.

Mulay, A., Konda, B., Garcia, G., Yao, C., Beil, S., Sen, C., Purkayastha, A., Kolls, J.K., Pociask, D.A., Pessina, P., *et al.* (2020). SARS-CoV-2 infection of primary human lung epithelium for COVID-19 modeling and drug discovery. bioRxiv, https://wwwbiorxivorg/content/101101/20200629174623v1.

Nickbakhsh, S., Mair, C., Matthews, L., Reeve, R., Johnson, P.C.D., Thorburn, F., von Wissmann, B., Reynolds, A., McMenamin, J., Gunson, R.N., *et al.* (2019). Virus-virus interactions impact the population dynamics of influenza and the common cold. Proceedings of the National Academy of Sciences of the United States of America.

Odendall, C., and Kagan, J.C. (2015). The unique regulation and functions of type III interferons in antiviral immunity. Curr Opin Virol *12*, 47-52.

Olsen, S.J., Azziz-Baumgartner, E., Budd, A.P., Brammer, L., Sullivan, S., Pineda, R.F., Cohen, C., and Fry, A.M. (2020). Decreased Influenza Activity During the COVID-19 Pandemic - United States, Australia, Chile, and South Africa, 2020. MMWR Morb Mortal Wkly Rep *69*, 1305-1309.

Onabajo, O.O., Banday, A.R., Stanifer, M.L., Yan, W., Obajemu, A., Santer, D.M., Florez-Vargas, O., Piontkivska, H., Vargas, J.M., Ring, T.J., *et al.* (2020). Interferons and viruses induce a novel truncated ACE2 isoform and not the full-length SARS-CoV-2 receptor. Nat Genet *52*, 1283-1293.

Pairo-Castineira, E., Clohisey, S., Klaric, L., Bretherick, A.D., Rawlik, K., Pasko, D., Walker, S., Parkinson, N., Fourman, M.H., Russell, C.D., *et al.* (2020). Genetic mechanisms of critical illness in Covid-19. Nature *https://www.nature.com/articles/s41586-020-03065-y*.

Pertea, M., Pertea, G.M., Antonescu, C.M., Chang, T.C., Mendell, J.T., and Salzberg, S.L. (2015). StringTie enables improved reconstruction of a transcriptome from RNA-seq reads. Nat Biotechnol *33*, 290-295.

Pfaender, S., Mar, K.B., Michailidis, E., Kratzel, A., Boys, I.N., V'Kovski, P., Fan, W., Kelly, J.N., Hirt, D., Ebert, N., *et al.* (2020). LY6E impairs coronavirus fusion and confers immune control of viral disease. Nat Microbiol *5*, 1330-1339.

Plasschaert, L.W., Zilionis, R., Choo-Wing, R., Savova, V., Knehr, J., Roma, G., Klein, A.M., and Jaffe, A.B. (2018). A single-cell atlas of the airway epithelium reveals the CFTR-rich pulmonary ionocyte. Nature *560*, 377-381.

Poole, S., Brendish, N.J., Tanner, A.R., and Clark, T.W. (2020). Physical distancing in schools for SARS-CoV-2 and the resurgence of rhinovirus. Lancet Respir Med *8*, e92-e93.

Prevention, C.f.D.C.a. (2020). CDC 2019-Novel Coronavirus (2019-nCoV) Real-Time RT-PCR Diagnostic Panel

Prevention, C.f.D.C.a. (2021). Emerging SARS-CoV-2 Variants.

Ravindra, N.G., Alfajaro, M.M., Gasque, V., Wei, J., Filler, R.B., Huston, N.C., Wan, H., Szigeti-Buck, K., Wang, B., Montgomery, R.R., *et al.* (2020). Single-cell longitudinal analysis of SARS-CoV-2 infection in human bronchial epithelial cells. bioRxiv.

764 Rusinova, I., Forster, S., Yu, S., Kannan, A., Masse, M., Cumming, H., Chapman, R., and Hertzog,
765 P.J. (2013). Interferome v2.0: an updated database of annotated interferon-regulated genes. Nucleic
766 Acids Res *41*, D1040-1046.
767 Schneider, W.M., Chevillotte, M.D., and Rice, C.M. (2014). Interferon-stimulated genes: a complex
768 web of host defenses. Annual review of immunology *32*, 513-545.
769 Schultz-Cherry, S. (2015). Viral Interference: The Case of Influenza Viruses. The Journal of infectious
770 diseases *212*, 1690-1691.
771 Singanayagam, A., Patel, M., Charlett, A., Lopez Bernal, J., Saliba, V., Ellis, J., Ladhani, S., Zambon,
772 M., and Gopal, R. (2020). Duration of infectiousness and correlation with RT-PCR cycle threshold values
773 in cases of COVID-19, England, January to May 2020. Euro Surveill *25*.
774 Stuart, T., Butler, A., Hoffman, P., Hafemeister, C., Papalexi, E., Mauck, W.M., 3rd, Hao, Y., Stoeckius,
775 M., Smibert, P., and Satija, R. (2019). Comprehensive Integration of Single-Cell Data. Cell *177*, 1888-
776 1902 e1821.
777 Taylor, J.K., Coleman, C.M., Postel, S., Sisk, J.M., Bernbaum, J.G., Venkataraman, T., Sundberg,
778 E.J., and Frieman, M.B. (2015). Severe Acute Respiratory Syndrome Coronavirus ORF7a Inhibits Bone
779 Marrow Stromal Antigen 2 Virion Tethering through a Novel Mechanism of Glycosylation Interference. J
780 Virol *89*, 11820-11833.
781 Vanderheiden, A., Ralfs, P., Chirkova, T., Upadhyay, A.A., Zimmerman, M.G., Bedoya, S., Aoued, H.,
782 Tharp, G.M., Pellegrini, K.L., Manfredi, C.*, et al.* (2020). Type I and Type III Interferons Restrict SARS-
783 CoV-2 Infection of Human Airway Epithelial Cultures. J Virol *94*, e00985-00920.
784 Vogels, C.B.F., Brito, A.F., Wyllie, A.L., Fauver, J.R., Ott, I.M., Kalinich, C.C., Petrone, M.E.,
785 Casanovas-Massana, A., Catherine Muenker, M., Moore, A.J.*, et al.* (2020). Analytical sensitivity and
786 efficiency comparisons of SARS-CoV-2 RT-qPCR primer-probe sets. Nat Microbiol *5*, 1299-1305.
787 Wang, N., Zhan, Y., Zhu, L., Zheng, Z., Lu, Y., Hong, P. (2020). Retrospective Multicenter Cohort
788 Study Shows Early Interferon Therapy Is Associated with Favorable Clinical Responses in COVID-19
789 Patients. Cell Host Microbe *28*, 455-464.
790 Wolsk, H.M., Folsgaard, N.V., Birch, S., Brix, S., Hansel, T.T., Johnston, S.L., Kebadze, T., Chawes,
791 B.L., Bonnelykke, K., and Bisgaard, H. (2016). Picornavirus-Induced Airway Mucosa Immune Profile in
792 Asymptomatic Neonates. The Journal of infectious diseases *213*, 1262-1270.
793 Wu, A., Mihaylova, V.T., Landry, M.L., and Foxman, E.F. (2020). Interference between rhinovirus and
794 influenza A virus: a clinical data analysis and experimental infection study. Lancet Microbe *1*, e254-e262.
795 Xia, H., Cao, Z., Xie, X., Zhang, X., Chen, J.Y., Wang, H., Menachery, V.D., Rajsbaum, R., and Shi,
796 P.Y. (2020). Evasion of Type I Interferon by SARS-CoV-2. Cell Rep *33*, 108234.
797 Yahya, M., Rulli, M., Toivonen, L., Waris, M., and Peltola, V. (2017). Detection of Host Response to
798 Viral Respiratory Infection by Measurement of Messenger RNA for MxA, TRIM21, and Viperin in Nasal
799 Swabs. The Journal of infectious diseases *216*, 1099-1103.
800 Yilmaz, A., Marklund, E., Andersson, M., Nilsson, S., Andersson, L.M., Lindh, M., and Gisslen, M.
801 (2020). Upper respiratory tract levels of SARS-CoV-2 RNA and duration of viral RNA shedding do not
802 differ between patients with mild and severe/critical COVID-19. The Journal of infectious diseases *223*,
803 15-18.
804 Yu, J., Peterson, D.R., Baran, A.M., Bhattacharya, S., Wylie, T.N., Falsey, A.R., Mariani, T.J., and
805 Storch, G.A. (2019). Host Gene Expression in Nose and Blood for the Diagnosis of Viral Respiratory
806 Infection. The Journal of infectious diseases *219*, 1151-1161.
807 Zhang, Q., Bastard, P., Liu, Z., Le Pen, J., Moncada-Velez, M., Chen, J., Ogishi, M., Sabli, I.K.D.,
808 Hodeib, S., Korol, C.*, et al.* (2020). Inborn errors of type I IFN immunity in patients with life-threatening
809 COVID-19. Science *370*, eabd4570.
810 Zheng, S., Fan, J., Yu, F., Feng, B., Lou, B., Zou, Q., Xie, G., Lin, S., Wang, R., Yang, X.*, et al.* (2020).
811 Viral load dynamics and disease severity in patients infected with SARS-CoV-2 in Zhejiang province,
812 China, January-March 2020: retrospective cohort study. BMJ *369*, m1443.

Zhou, Z., Ren, L., Zhang, L., Zhong, J., Xiao, Y., Jia, Z., Guo, L., Yang, J., Wang, C., Jiang, S*., et al.* (2020). Heightened Innate Immune Responses in the Respiratory Tract of COVID-19 Patients. Cell Host Microbe *27*, 883-890 e882.

Ziegler, C.G.K., Allon, S.J., Nyquist, S.K., Mbano, I.M., Miao, V.N., Tzouanas, C.N., Cao, Y., Yousif, A.S., Bals, J., Hauser, B.M*., et al.* (2020). SARS-CoV-2 Receptor ACE2 Is an Interferon-Stimulated Gene in Human Airway Epithelial Cells and Is Detected in Specific Cell Subsets across Tissues. Cell *181*, 1016-1035 e1019.

Figures

Fig 1. Transcriptome analysis of RNA isolated from SARS-CoV-2+ nasopharyngeal swabs

Fig 2. Relationship between nasopharyngeal (NP) CXCL10 and viral load in 140 SARS-CoV-2+ patients.

Fig 3. Viral load and nasopharyngeal CXCL10 patterns in vivo over time

Fig 4. Kinetics of SARS-CoV-2 replication in organoids and in vivo.

Fig 5. Effect of prior rhinovirus infection on ISG induction and SARS-CoV-2 replication in human airway epithelial organoids.

Fig 6. Effect of blocking ISG induction on SARS-CoV-2 replication following rhinovirus infection.

Fig 7. Effect of blocking ISG induction on SARS-CoV-2 replication in a low MOI infection

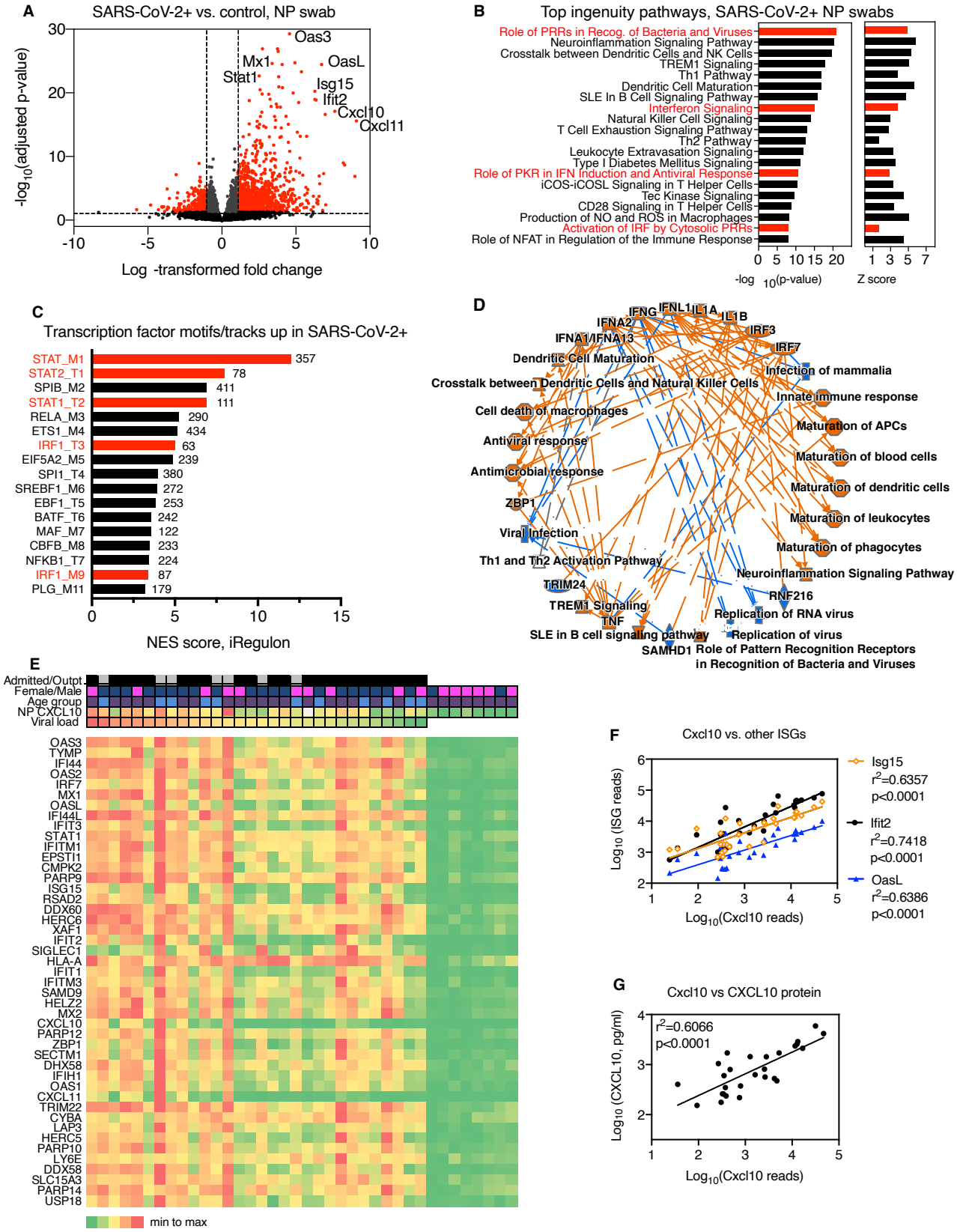

Fig 1. Transcriptome analysis of RNA isolated from SARS-CoV-2+ nasopharyngeal swabs.

Fig 1. Transcriptome analysis of RNA isolated from SARS-CoV-2+ nasopharyngeal swabs (related to Fig S1).

(A) Volcano plot showing significantly differentially expressed protein-coding genes based on RNASeq of NP swab RNA from SARS-CoV-2 patients (n=30) compared to control SARS-CoV-2 negative subjects (n=8). Transcripts with fold change>2, adjusted p-value<0.05 are highlighted in red.

(B) Top 20 ingenuity pathways enriched in SARS-CoV-2+ compared to controls, based on 1770 differentially expressed RNAs. P-value and Z-score for each pathway is indicated on the x-axis. Pathways related to interferon and interferon regulatory factor (IRF) signaling are highlighted in red.

(C) Transcription factor binding sites associated with NP transcripts enriched in SARS-CoV-2+ patients compared to controls. Bars show strength of association of motifs/tracks with enriched transcripts, indicated by NES score. Y-axis label indicates top transcription factor associated with each cluster of motifs (M) or tracks (T) and the cluster code. Number of enriched transcripts associated with each track/motif is indicated to the right of each bar. Transcription factors associated with the interferon response are highlighted in red.

(D) Graphical summary of pathways and regulators enriched based on ingenuity pathway analysis of differentially expressed genes enriched in NP RNA of SARS-CoV-2+ patients compared to controls.

(E) Heatmap showing relative expression level of top 45 most significant differentially expressed genes in patients (left) or SARS-CoV-2-negative controls (right). Clinical characteristics of each patient are indicated by color: viral load (red=highest viral load/lowest Ct value, green=lowest viral load/highest Ct value); NP CXCL10 protein level (red=highest, green=lowest, white=data not available). Heatmap colors represent values from highest (red) to lowest (green) for viral load (based on Ct value), CXCL10 concentration (pg/ml), or gene expression level, scaled from minimum to maximum (green=0; yellow=0.5, red=1) Patient characteristics indicated at the top of the graph include Admission status (grey=outpatient, black= admitted); Gender (blue=male, pink=female); Age (blue<55yrs, purple>60 yrs.) White = data not available.

(F) Correlation between reads mapping to CXCL10 and reads mapping to other ISGs (Ifit2, OasL, Isg15).

(G) Correlation between reads mapping to Cxcl10 and CXCL10 protein measured by ELISA in NP swab-associated viral transport medium.

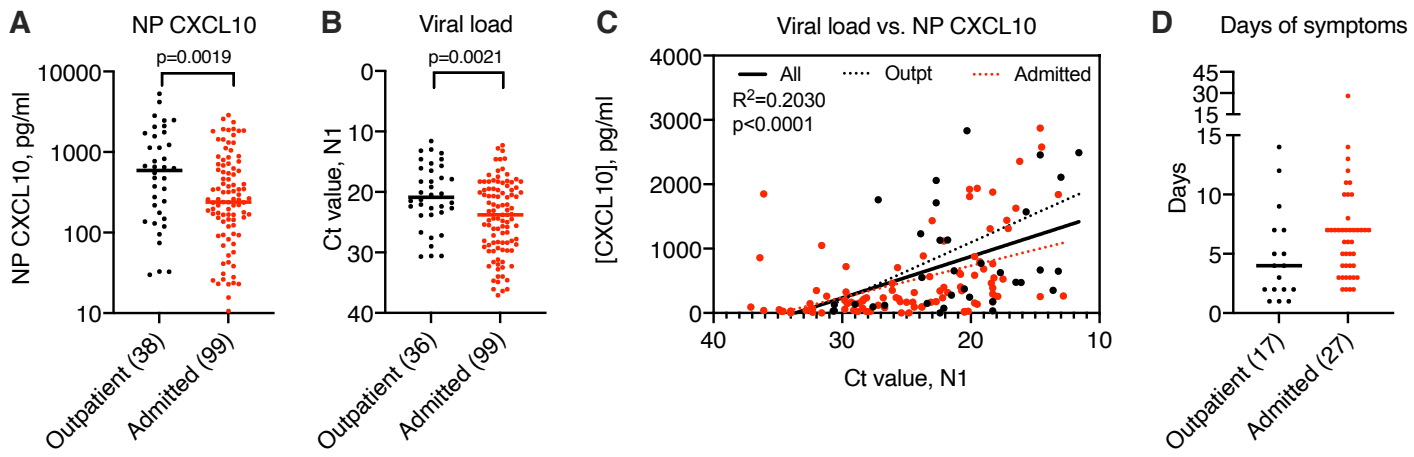

Fig 2 (related to Fig S2). Relationship between nasopharyngeal (NP) CXCL10 and viral load in 140 SARS-CoV-2+ patients.

(A) NP CXCL10 level in patients testing positive for SARS-CoV-2 by RT-qPCR at Yale-New Haven Hospital in March 2020. Black symbols indicate patients tested as outpatients or in the emergency department and not admitted to the hospital, red symbols indicate patients admitted to the hospital.

(B) Ct value for SARS-CoV-2 N1 gene in outpatients and admitted patients. Number in parenthesis (A, B) indicates number of outpatient (total n=38) and admitted (total n=102) samples for which data was available.

(C) Regression analysis showing relationship between viral load and NP CXCL10 protein for all samples (black solid line, r^2 and p-value indicated) or for only outpatients (dashed black line) or admitted patients (dotted red line).

(D) Days of symptoms reported prior to testing for samples with this information available (number indicated n parentheses).

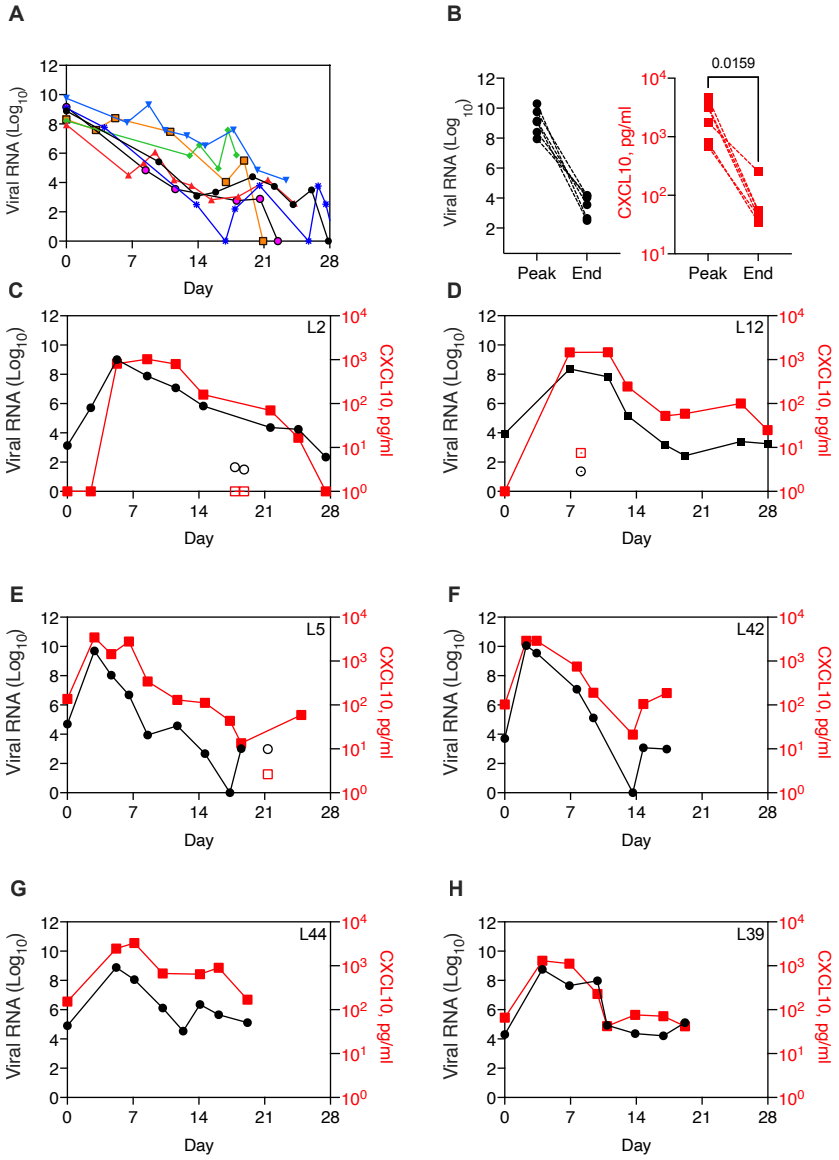

Fig 3 (related to Table S1). Nasopharyngeal viral load and CXCL10 in patients diagnosed prior to peak viral load.

(A) Viral load over time in seven longitudinal samples from patients with high viral load in first sample (Ct N1>20).

(B) Paired viral RNA and NP CXCL10 measurements at the peak viral load and at the end viral load, defined as the first sample with Ct N1>30, for 6 patients shown in (G) (data not available for one sample). CXCL10 level was significantly different in peak and end samples by paired t-test.

(C) – (H) Viral load and NP CXCL10 level in longitudinal samples from SARS-CoV-2+ patients who presented with a low viral load (Ct N1>28) that increased to a high viral load (Ct N1<20). Viral load is expressed as fold change from the limit of detection for the SARS-CoV-2 N1 gene (black circles) and CXCL10 is expressed as pg/ml in the NP-swab associated viral transport medium (red squares). Samples with low levels of RnaseP, an indicator of sample quality, are shown with open symbols. Patient characteristics are described in Table S5.

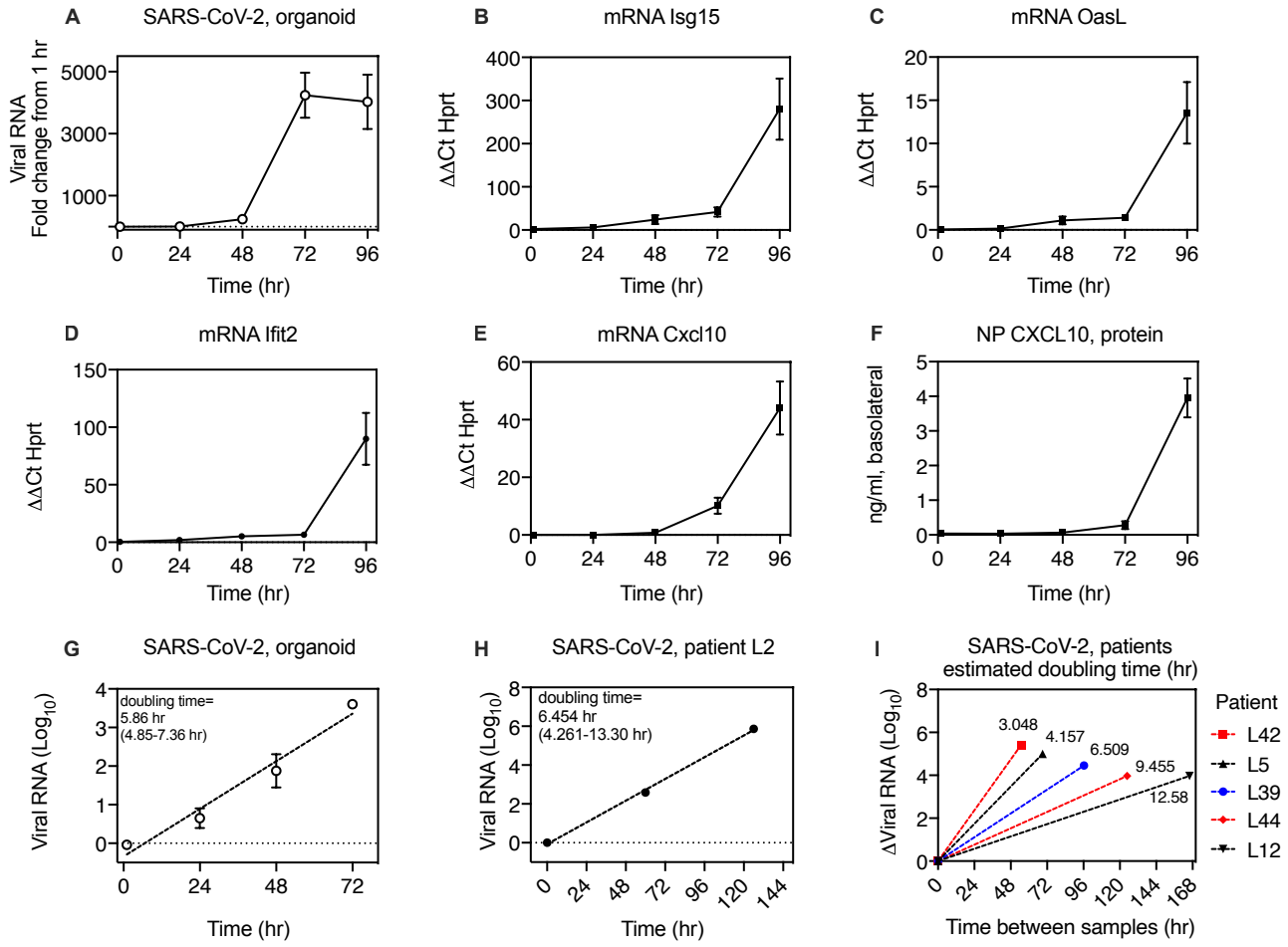

Figure 4. Kinetics of SARS-CoV-2 replication in organoids and in vivo.

(A) Time course of SARS-CoV-2 replication in human primary airway epithelial organoids, expressed as fold increase from 1hr (post-inoculation time point).

(B) - (E) ISG mRNA level relative to HPRT mRNA in organoids during SARS-CoV-2 infection.

(F) CXCL10 protein in the basolateral medium during SARS-COV-2 replication. For A-H, symbols show mean and S.E.M. of five biological replicates per condition.

(G) Exponential curve fit for increase in RNA during SARS-CoV-2 during replication in organoids from 1-72 hr and calculated doubling time for exponential growth.

(H) Exponential curve fit for increase in viral RNA during SARS-CoV-2 replication for first three virus-positive samples from patient L2 and calculated doubling time for exponential growth with 95% confidence interval.

(I) Estimated doubling times for increase in viral RNA during SARS-CoV-2 replication in patients with one SARS-CoV-2 positive sample prior to peak viral load, shown in fig 3 B-F. Y-axis shows change in viral RNA and x-axis shows time interval between samples. Doubling time calculation assumes exponential growth between first and peak viral load samples.

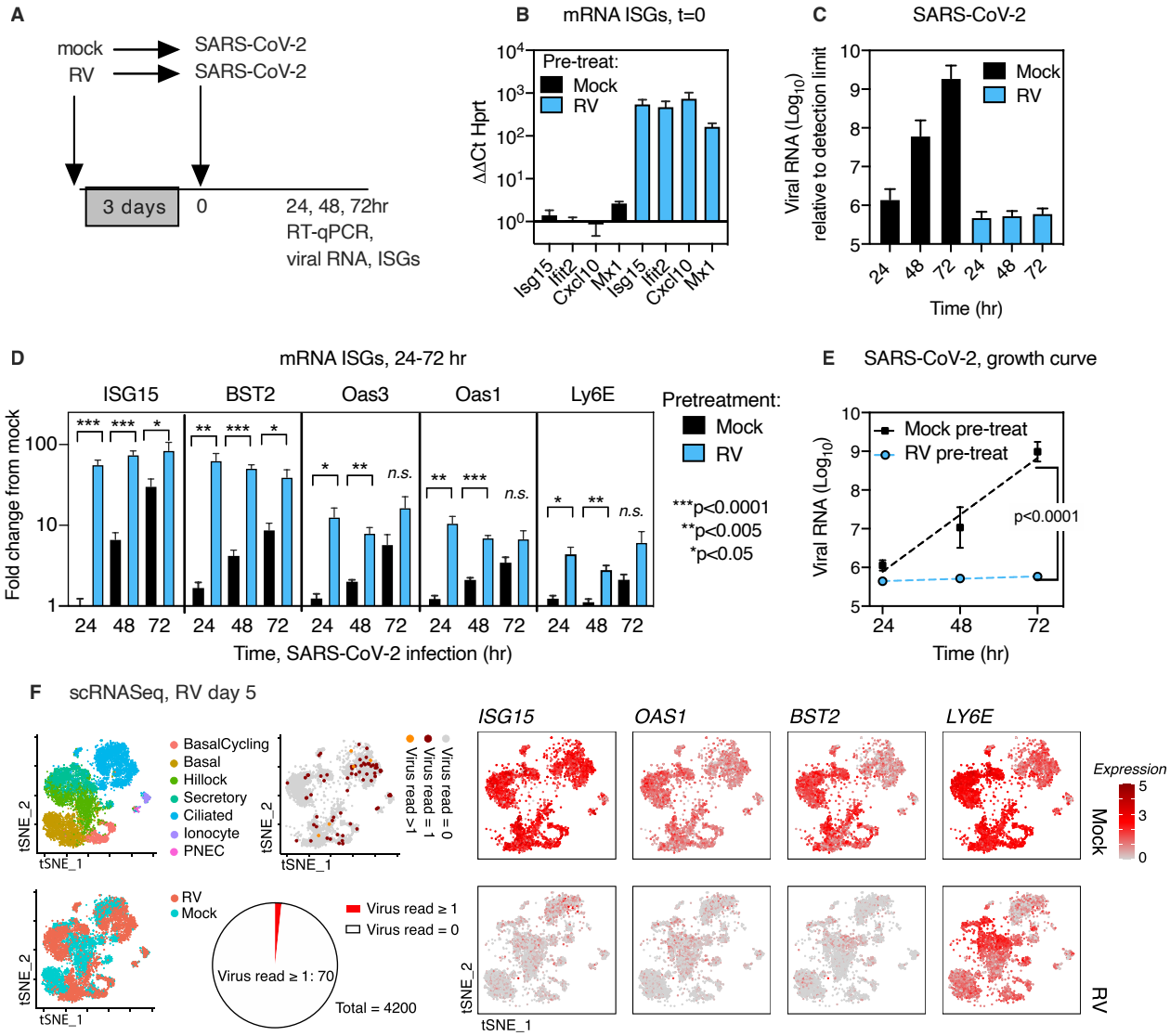

Figure 5. Effect of prior rhinovirus infection on ISG induction and SARS-CoV-2 replication in human airway epithelial organoids.

(A) Timing of infection of epithelial organoids with rhinovirus followed by SARS-CoV-2
(B) Expression of interferon stimulated genes in airway epithelial organoids 3 days post-rhinovirus infection, relative to mRNA for the housekeeping gene HPRT
(C) SARS-CoV-2 viral RNA at 24, 48, and 72 hr post-infection, with or without RV pre-infection
(D) Expression of interferon stimulated genes at 24, 48, and 72 hr post SARS-CoV-2 infection, with or without RV pre-infection, expressed as fold change from uninfected cells
(E) Replication of SARS-CoV-2 in mock- vs. rhinovirus-pretreated cultures, fit to exponential growth curve
(F) Single cell sequencing of human airway epithelial cell organoids, mock or 5 days post rhinovirus infection. Red and orange dots indicate 70/4200 cells with detectable viral RNA at this time point in rhinovirus-infected cultures (at least 1 read from viral RNA). TSNE plots show expression of mRNA for ISGs in mock and infected cultures at the same time point.

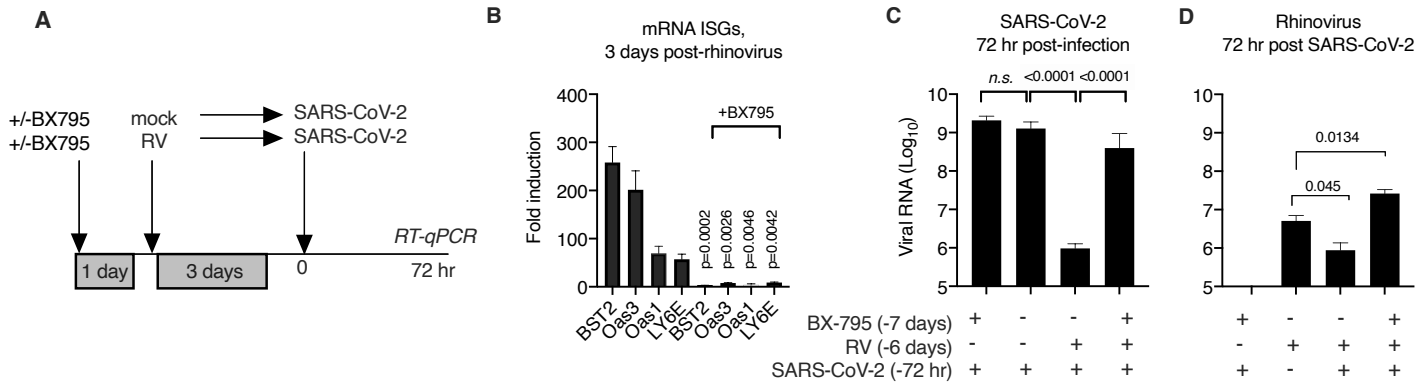

Figure 6. Effect of pretreatment with BX795 during sequential rhinovirus, SARS-CoV-2 infection

Organoid cultures were pretreated with or without BX795 for 18 hr, then mock-infected or infected with HRV01A, incubated for 3 days, then infected with SARS-CoV-2.

(A) Effect of BX-795 pre-treatment on ISG induction, 3 days post rhinovirus infection. Bars show fold change in ISG mRNA level in RV infected cultures compared to mock without (left) or with (right) BX-795 pre-treatment. P values indicate significant differences between ISG levels in cultures with or without BX795 pretreatment by t-test.

(B) SARS-CoV-2 viral RNA level relative to the limit of detection in organoid cultures, 72 hr post SARS-CoV-2 infection, with and without BX-795 and/or RV pre-treatment. P values indicate significant differences in viral RNA levels, n.s. = not significant.

(C) HRV01A viral RNA level relative to the limit of detection in organoid cultures, 72 hr post SARS-CoV-2 infection, with and without BX-795 and/or RV pre-treatment. This graph also includes cultures infected with RV but not subsequently infected with SARS-CoV-2. P values indicate significant differences in viral RNA levels.

For all graphs, bars show mean and S.E.M. of 4-6 biological replicates per condition.

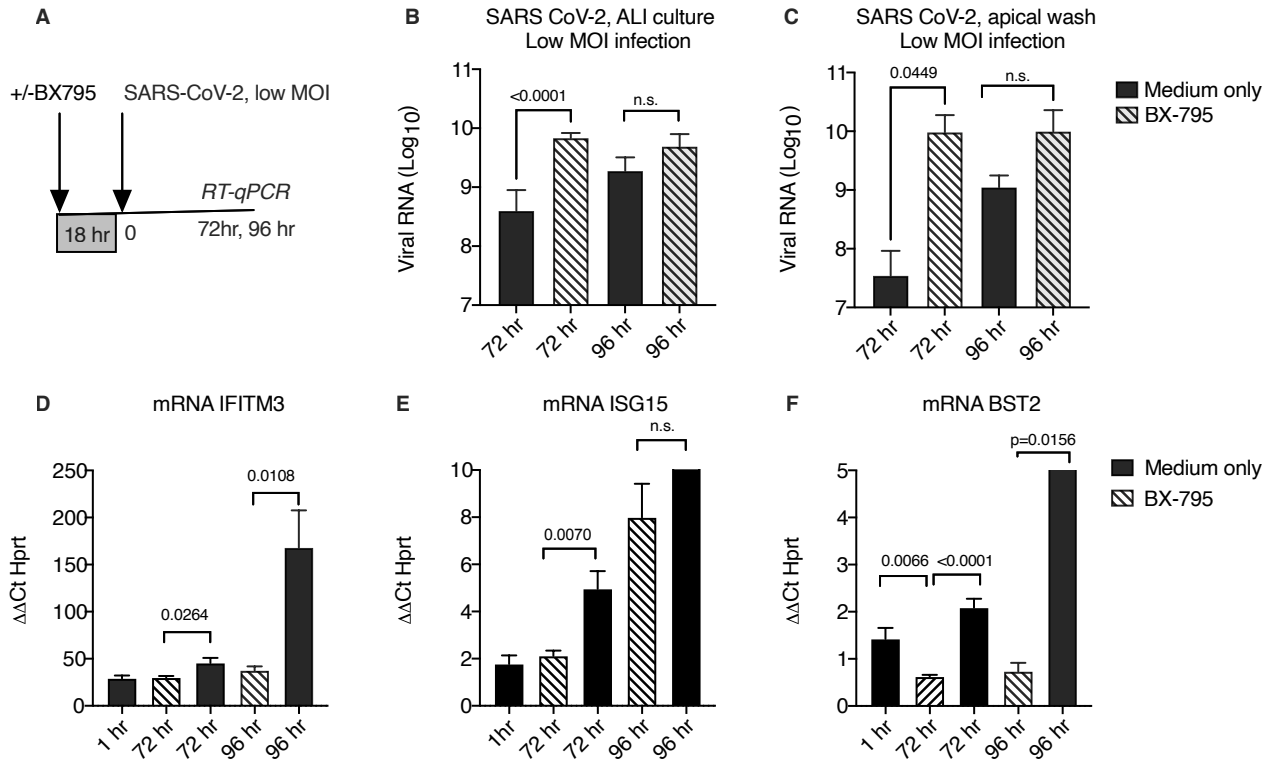

Fig 7. Effect of BX795 on SARS-CoV-2 replication in low MOI infection

(A) Cultures were pre-treated with 6μM BX-795 or medium only, then inoculated with SARS-CoV-2, MOI 0.05, at t=0 hr. Cultures were collected for RNA isolation and RT-qPCR at t=1, 72, and 96 hr post infection. Apical wash was collected at 72 and 92 hr post-infection.

(B)SARS-CoV-2 viral RNA in RNA isolated from organoid cultures 72 hr and 96 hr post-inoculation, with (hatched bars) or without BX795 (black bars), relative to the limit of detection.

(C)SARS-CoV-2 viral RNA in RNA isolated from the apical wash of cultures collected at 72 hr and 96 hr post-inoculation, with (hatched bars) or without BX795 (black bars), relative to the limit of detection.

(D)-(F) ISG mRNA level in SARS-CoV-2 infected cultures, graphed relative to the mRNA level for the housekeeping gene HPRT ($2^{Ct-Ct\ HPRT}$), at 1, 72, or 96 hr post-inoculation.

(B)-(F) Bars show mean and S.E.M. for 4-6 biological replicates per condition. P-values are shown for significant differences, based on the students t-test.